Gastroenterology 2021;160:1284–1300

RNA N^6-Methyladenosine Methyltransferase METTL3 Facilitates Colorectal Cancer by Activating the m^{6}A-GLUT1-mTORC1 Axis and Is a Therapeutic Target

Huarong Chen,[1] Shanshan Gao,[1] Weixin Liu,[1] Chi-Chun Wong,[1] Jianfeng Wu,[2] Jingtong Wu,[2] Dabin Liu,[1] Hongyan Gou,[1] Wei Kang,[3] Jianning Zhai,[1] Chuangen Li,[1] Hao Su,[1] Shiyan Wang,[4] Fraser Soares,[4] Jiahuai Han,[2] Housheng Hansen He,[4] and Jun Yu[1]

[1]Institute of Digestive Disease and Department of Medicine and Therapeutics, State Key laboratory of Digestive Disease, Li Ka Shing Institute of Health Sciences, Shenzhen Research Institute, The Chinese University of Hong Kong, Hong Kong; [2]State Key Laboratory of Cellular Stress Biology and School of Life Sciences, Xiamen University, Xiamen, China; [3]Department of Anatomical and Cellular Pathology, State Key Laboratory of Oncology in South China, Prince of Wales Hospital, The Chinese University of Hong Kong, Hong Kong; and [4]Princess Margaret Cancer Centre, University Health Network, Department of Medical Biophysics, University of Toronto, Toronto, Canada

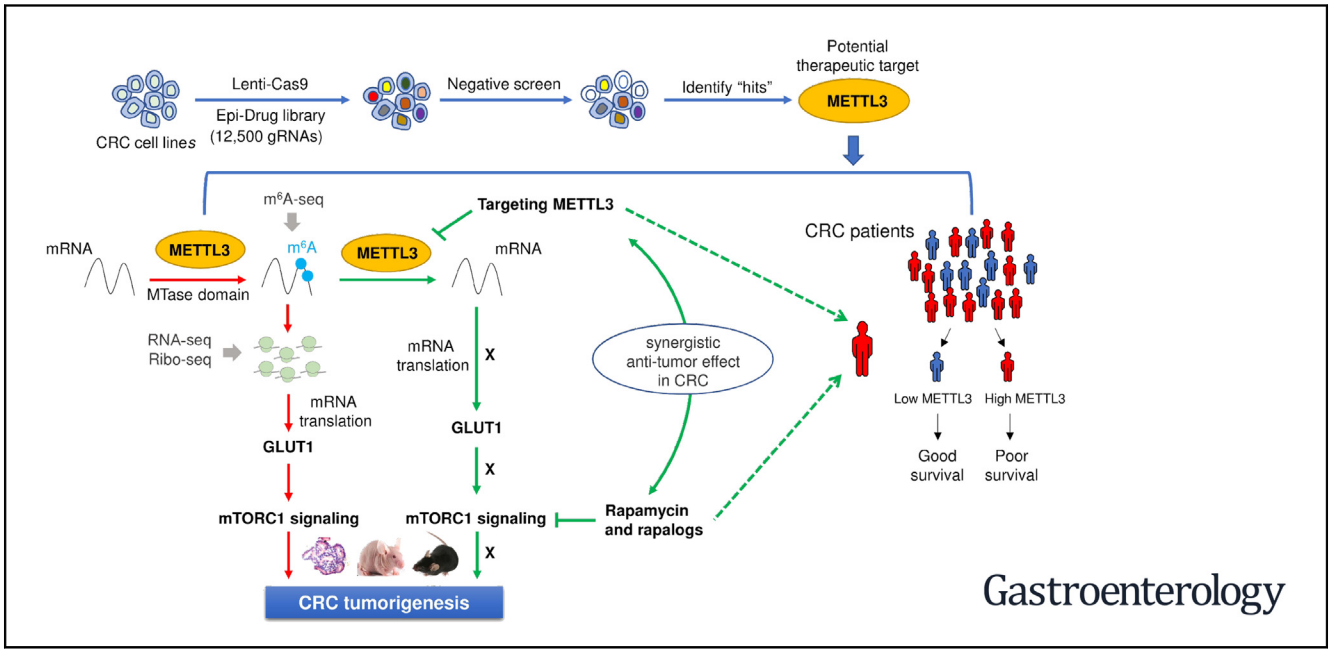

BACKGROUND & AIMS: RNA N^6-methyladenosine (m^{6}A) modification has recently emerged as a new regulatory mechanism in cancer progression. We aimed to explore the role of the m^{6}A regulatory enzyme METTL3 in colorectal cancer (CRC) pathogenesis and its potential as a therapeutic target. **METHODS:** The expression and clinical implication of METTL3 were investigated in multiple human CRC cohorts. The underlying mechanisms of METTL3 in CRC were investigated by integrative m^{6}A sequencing, RNA sequencing, and ribosome profiling analyses. The efficacy of targeting METTL3 in CRC treatment was elucidated in CRC cell lines, patient-derived CRC organoids, and *Mettl3*-knockout mouse models. **RESULTS:** Using targeted clustered regularly interspaced short palindromic repeats (CRISPR)/Cas9 dropout screening, we identified METTL3 as the top essential m^{6}A regulatory enzyme in CRC. METTL3 was overexpressed in 62.2% (79/127) and 88.0% (44/50) of primary CRCs from 2 independent cohorts. High METTL3 expression predicted poor survival in patients with CRC (n = 374, $P < .01$). Functionally, silencing METTL3 suppressed tumorigenesis in CRC cells, human-derived primary CRC organoids, and Mettl3-knockout mouse models. We discovered the novel functional m^{6}A methyltransferase domain of METTL3 in CRC cells by domain-focused CRISPR screening and mutagenesis assays. Mechanistically, METTL3 directly induced the m^{6}A-GLUT1-mTORC1 axis as identified by integrated m^{6}A sequencing, RNA sequencing, ribosome sequencing, and functional validation. METTL3 induced GLUT1 translation in an m^{6}A-dependent manner, which subsequently promoted glucose uptake and lactate production, leading to the activation of mTORC1 signaling and CRC development. Furthermore, inhibition of mTORC1 potentiated the anticancer effect of METTL3 silencing in CRC patient–derived organoids and

METTL3 transgenic mouse models. **CONCLUSIONS:** METTL3 promotes CRC by activating the m^{6}A-GLUT1-mTORC1 axis. METTL3 is a promising therapeutic target for the treatment of CRC.

Keywords: Colorectal Cancer; *N*^{6}-Methyladenosine; Glucose Metabolism; mTORC1.

WHAT YOU NEED TO KNOW

BACKGROUND AND CONTEXT

N^6-methyladenosine (m^{6}A) modification has recently emerged as a new regulatory mechanism in cancer progression. However, whether and how m^{6}A modifications can translate to a pro-tumorigenic signal in colorectal cancer (CRC) is largely unclear.

NEW FINDINGS

METTL3 is an essential m^{6}A regulator enzyme in colorectal carcinogenesis. Functionally, METTL3 promotes CRC initiation and progression through inducing a novel m^{6}A-GLUT1-mTORC1 axis. Conserved motifs (DPPW, IHM and RTGRTGH) among MTase domain are important for METTL3 function in CRC. Inhibition of mTORC1 potentiates the anticancer effect of METTL3 silencing in CRC.

LIMITATIONS

This study does not take the effect of METTL3 on tumor microenvironment into consideration.

IMPACT

High METTL3 expression is a poor prognostic factor and potential therapeutic target for CRC patients.

RNA *N*^{6}-methyladenosine (m^{6}A) is the most abundant RNA modification in the human and a key determinant in posttranscriptional regulation of messenger RNA (mRNA) splicing, translation, and degradation.[1,2] Emerging studies have unveiled a critical role of RNA m^{6}A modification by RNA modification enzymes in the fine-tuning of gene expression.[1] Aberrant m^{6}A regulation was recently shown to play multifaceted roles in tumorigenesis; however, the causality of m^{6}A in cancer development remains poorly understood. RNA m^{6}A modification undergoes dynamic regulation through methylation by writers, recognition by readers, and demethylation by erasers. Deregulated expression of m^{6}A regulatory enzymes has been shown to promote tumorigenesis, metastasis, and cancer stem cell self-renewal.[3–7] Targeting m^{6}A RNA methylation regulators have also shown promise in preclinical models, as exemplified by inhibitors of the m^{6}A eraser FTO, which are effective in the treatment of acute myeloid leukemia.[8] Nevertheless, whether and how m^{6}A modifications can translate to a pro-tumorigenic signal in colorectal cancer (CRC) is largely unclear.

To explore the role of m^{6}A regulatory enzymes important in CRC pathogenesis and uncover drug targets, we performed a clustered regularly interspaced short palindromic repeats (CRISPR)/Cas9 library screening in CRC cell lines and revealed METTL3, an m^{6}A methyltransferase, as the top essential gene for CRC cell survival. In this study, we investigated the functional significance and underlying mechanisms of METTL3 as an m^{6}A methyltransferase in colorectal carcinogenesis using integrative m^{6}A-sequencing (m^{6}A-seq), RNA sequencing (RNA-seq), and ribosome profiling (Ribo-seq) analyses, and we identified associations between METTL3-mediated m^{6}A modification, RNA metabolism, and oncogenic signal transduction in CRC cells, patient-derived CRC organoids, and animal models. We further elucidated the efficacy of targeting METTL3-mediated m^{6}A modification in CRC.

Materials and Methods

Human Colorectal Samples

Five cohorts of patients with colorectal cancer were included. Cohort 1 from the Beijing University Cancer Hospital comprised 127 patients with CRC with surgically excised CRC tissues and surrounding nontumor tissues. Specimens were immediately snap frozen in liquid nitrogen and then stored at –80°C until further processing. Cohort 2 was The Cancer Genome Atlas (TCGA) cohort, consisting of METTL3 mRNA expression data from 50 pairs of CRC samples and nontumor tissues.[9] Cohort 3 from the Chinese University of Hong Kong consisted of 197 patients with CRC with surgically excised CRC tissues. Patients from cohort 3 were followed up regularly with available patient information, and the median follow-up time was 61.1 months (range, 0.13–182 months). For cohort 4, METTL3 mRNA expression from 177 CRC tumors and patient information were acquired from the Gene Expression Omnibus (GSE17536, https://www.ncbi.nlm.nih.gov/gds), and the median follow-up time was 42.3 months (range, 0.92–143 months). Cohort 5 was from the GSE100179 data set involving 20 healthy colonic, 20 colorectal adenoma, and 20 CRC tissues. The clinicopathologic features of patients are provided in Supplementary Tables 1 and 2. Informed consent was obtained for all patients, and this study was approved by the ethics

Abbreviations used in this paper: **4E-BP1, eukaryotic translation initiation factor 4E-binding proteins 1; AA, amino acid; AOM, azoxymethane; CI, confidence interval; CMS, consensus molecular subtype; CRC, colorectal cancer; CRISPR, clustered regularly interspaced short palindromic repeats; DSS, dextran sulfate sodium; EV, empty vector; GFP, green fluorescent protein; GLUT1, glucose transporter 1; HR, hazard ratio; IHC, immunohistochemistry; m^{6}A, *N*^{6}-methyladenosine, m^{6}A-seq, *N*^{6}-methyladenosine sequencing; MeRIP, methylated RNA immunoprecipitation; mRNA, messenger RNA; MSI, microsatellite instability; mTORC1, mammalian target of rapamycin complex 1; MTase, methyltransferase; mut, mutant; qPCR, quantitative polymerase chain reaction; Ribo-seq, ribosome profiling; RNA-seq, RNA-sequencing; RPF, ribosome protected fragment; sgRNA, single-guide RNA; shRNA, short hairpin RNA; S6K1, ribosomal protein S6 kinase beta-1; TCGA, The Cancer Genome Atlas; TEM, temsirolimus; TUNEL, terminal deoxynucleotidyl transferase–mediated deoxyuridine triphosphate nick-end labeling; UTR, untranslated region; WT, wild type.**

Most current article

0016-5085
https://doi.org/10.1053/j.gastro.2020.11.013

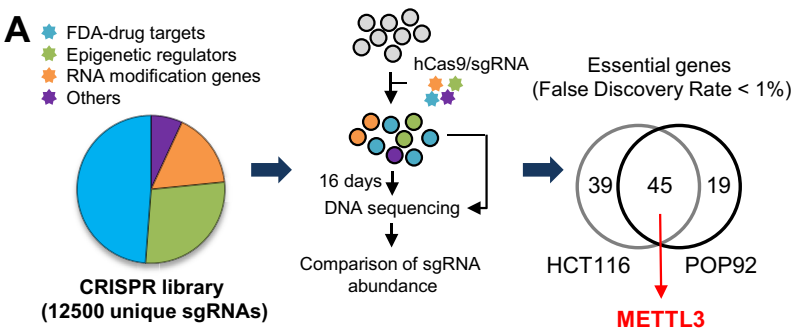
A
FDA-drug targets
Epigenetic regulators
RNA modification genes
Others
CRISPR library
(12500 unique sgRNAs)
hCas9/sgRNA
16 days
DNA sequencing
Comparison of sgRNA abundance
Essential genes
(False Discovery Rate < 1%)
39
45
19
HCT116
POP92
METTL3

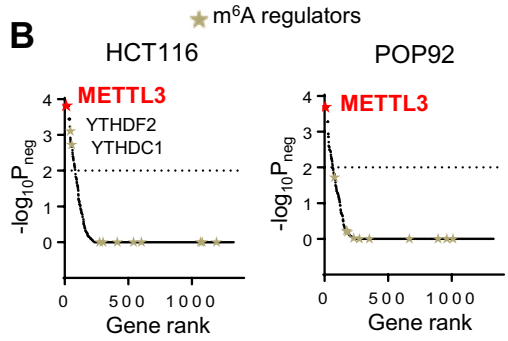
B
m6A regulators
HCT116
POP92
METTL3
YTHDF2
YTHDC1
-log10Pneg
Gene rank

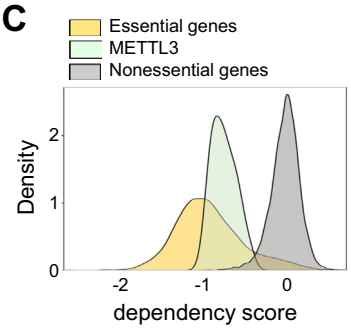
C
Essential genes
METTL3
Nonessential genes
Density
dependency score

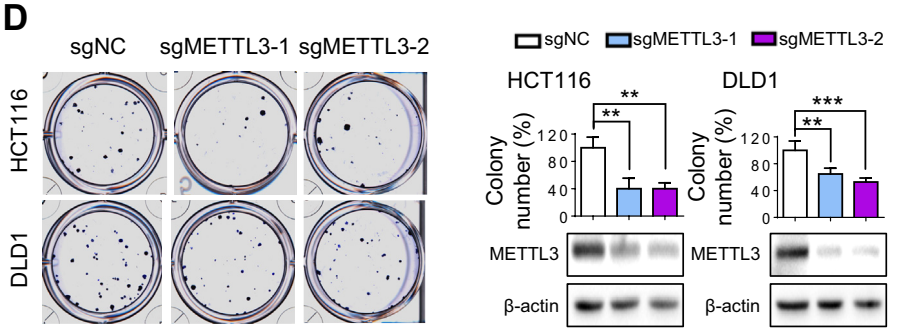
D
sgNC
sgMETTL3-1
sgMETTL3-2
HCT116
DLD1
Colony number (%)
METTL3
β-actin

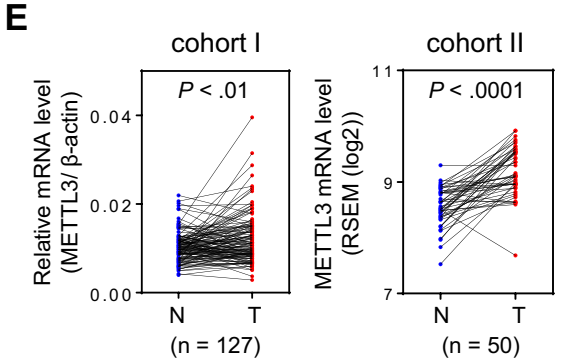
E
cohort I
cohort II
P < .01
P < .0001
Relative mRNA level (METTL3/ β-actin)
METTL3 mRNA level (RSEM (log2))
N
T
(n = 127)
(n = 50)

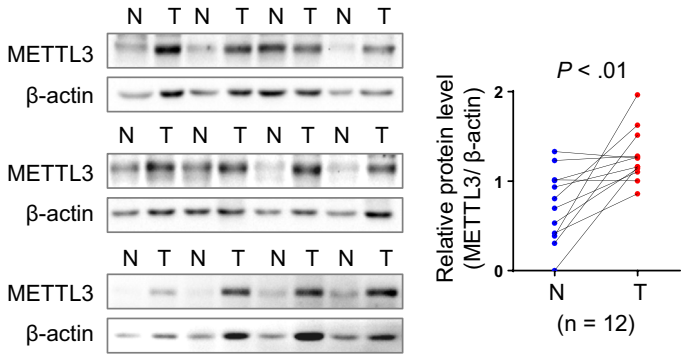
F
METTL3
β-actin
Relative protein level (METTL3/ β-actin)
P < .01
(n = 12)

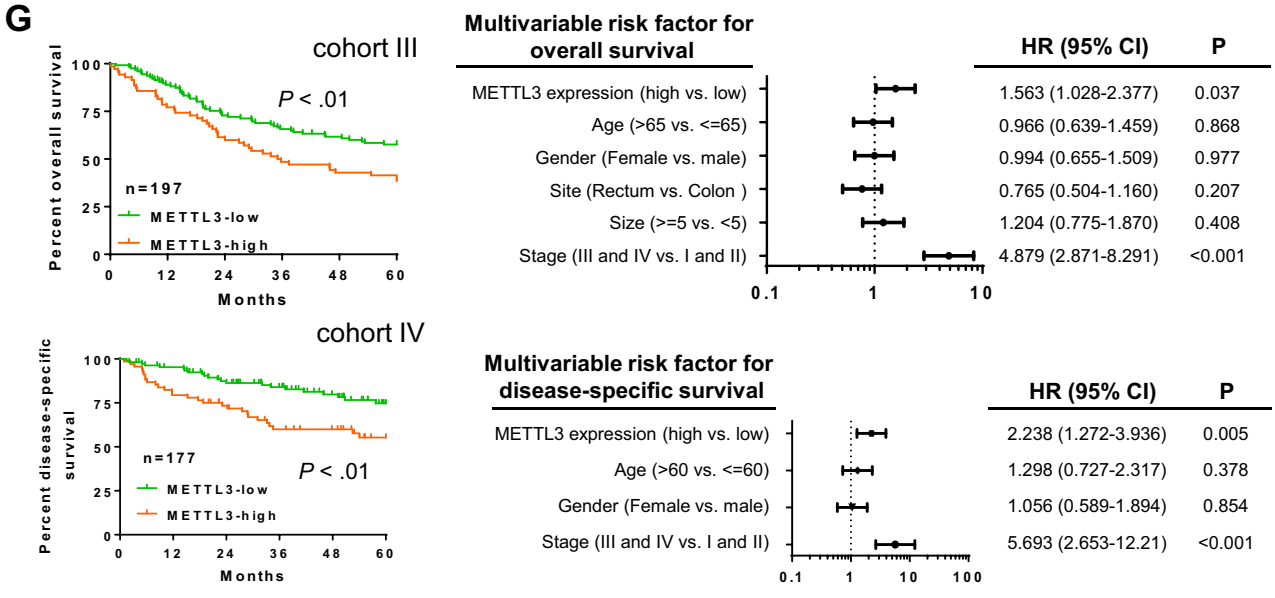
G
cohort III
P < .01
n=197
METTL3-low
METTL3-high
Percent overall survival
Months
Multivariable risk factor for overall survival
METTL3 expression (high vs. low)
Age (>65 vs. <=65)
Gender (Female vs. male)
Site (Rectum vs. Colon)
Size (>=5 vs. <5)
Stage (III and IV vs. I and II)
HR (95% CI)
P
1.563 (1.028-2.377) 0.037
0.966 (0.639-1.459) 0.868
0.994 (0.655-1.509) 0.977
0.765 (0.504-1.160) 0.207
1.204 (0.775-1.870) 0.408
4.879 (2.871-8.291) <0.001
cohort IV
n=177
P < .01
Percent disease-specific survival
Multivariable risk factor for disease-specific survival
METTL3 expression (high vs. low)
Age (>60 vs. <=60)
Gender (Female vs. male)
Stage (III and IV vs. I and II)
2.238 (1.272-3.936) 0.005
1.298 (0.727-2.317) 0.378
1.056 (0.589-1.894) 0.854
5.693 (2.653-12.21) <0.001

committee of the Chinese University of Hong Kong and the Beijing University Cancer Hospital.

Transgenic Mouse Model

To generate the *Mettl3*$^{+/-}$ mice, 2 specific single-guide RNAs (sgRNAs) targeting exon 2 of Mettl3 were used, which resulted in a frameshift mutation and generated a premature stop codon. The animals were maintained on a C57BL/6 background. Mice of 7–8 weeks old were injected intraperitoneally with azoxymethane (AOM) (10 mg/kg body weight) (Sigma-Aldrich). Five days later, mice were given 1.5% dextran sulfate sodium (DSS) (MP Biomedicals) in drinking water for 4 days followed by 2 weeks of regular drinking water. DSS treatments were repeated twice, and mice were killed on day 80. Meanwhile, *Mettl3*$^{+/-}$ mice were bred to *Apc*$^{Min/+}$ mice to generate *Apc*$^{Min/+}$*Mettl3*$^{+/-}$ mice. Only male mice were used in this study. All animal studies were performed in accordance with the guidelines approved by the Animal Experimentation Ethics Committee of The Chinese University of Hong Kong and Xiamen University.

N^6-Methyladenosine Sequencing

m^{6}A-seq was performed as described in a previous publication.[10] RNA was extracted by using Trizol reagent (Thermo Fisher Scientific) and treated with DNase I (Roche Diagnostics) to remove DNA contamination. RNA was subjected to fragmentation and then incubated with anti-m^{6}A antibody (Merck Millipore). The antibody-RNA complexes were bound to chromatin immunoprecipitation–grade Protein A/G Magnetic Beads (Merck Millipore) and washed by using the low/high salt-washing method. The m^{6}A-enriched RNA was eluted from the beads, purified by using RNeasy Mini Kit (Qiagen), and then sent for sequencing with the Illumina PE150, following the protocol from company (Novogene). For methylated RNA immunoprecipitation (MeRIP)–quantitative polymerase chain reaction (qPCR), m^{6}A-enriched RNA was reverse-transcribed by using the High-Capacity cDNA Reverse Transcription Kit (Thermo Fisher Scientific). The enrichment of m^{6}A-containing transcripts was determined by qPCR. The primers used are listed in Supplementary Table 3. The m^{6}A Viewer software was used to analyze the m^{6}A peaks from sequencing data.[11] The 5′ untranslated region (UTR), coding sequence, and 3′ UTR of each transcript were normalized to the same length, and the global profile of m^{6}A peaks was evaluated. The m^{6}A motif was identified through DREME (http://meme-suite.org/tools/dreme) analysis. The differential m^{6}A level was analyzed accordingly.[10] Integrative Genomics Viewer, version 2.3.94, was used for visualizing selected genes.

RNA Sequencing

RNA was extracted and treated with DNase I. After passing quality control, the libraries were generated and sequenced with the Illumina HiSeq 4000 (PE150) according to the protocol from the company (Epibiotek). RNA-seq reads were preceded by removing adapters using cutadapt, version 1.18, and mapped on the human reference (GENCODE, version 30) by HISAT2, version 2.1.0, with the default options. The number of reads mapped to each of genes was counted by using HTSeq, version 0.11.2, with the option -m intersection-nonempty. Gene expression levels were calculated as fragments per kilobase of transcript per million mapped reads by using DESeq2.[12]

Ribosome Profiling

The Ribo-seq strategy was followed as described in a previous publication.[13] Cells were treated with 100 μg/mL cycloheximide for 5 minutes at 37°C before collection. The cells were then lysed and treated with RNAse I to degrade unprotected mRNA regions. The intact mRNA-ribosome complexes were isolated and sent for sequencing with the Illumina HiSeq 4000 (SE50), following the protocol from company (Epibiotek). Reads were preceded by removing adapters. Reads mapping on human ribosomal RNA, small nucleolar RNA, small nuclear RNA, and transfer RNA from the GENCODE project, version 30, were discarded. The remaining reads were mapped on the human genome by bowtie2, version 2.3.4.3, with option -L 10. The expression levels of protein-coding genes were calculated by featureCounts, version 1.6.4, with the following parameters: –M ––fracOverlap 0.4 –largestOverlap.

Results

Clustered Regularly Interspaced Short Palindromic Repats/Cas9 Library Screening Identifies METTL3 as a Drug Target in Colorectal Cancer

To identify novel genes essential for CRC in an unbiased manner, we performed CRISPR/Cas9 dropout screening in 2 CRC cell lines (HCT116 and POP92) (Figure 1*A*). Overlap of gene candidates in HCT116 and POP92 cells showed 45 common druggable target genes (false discovery rate, <1%) (Figure 1*A*). Among them, METTL3, a m^{6}A

Figure 1. METTL3 is essential for CRC growth and predicts poor prognosis in patients with CRC. (*A*) The composition of our CRISPR library and workflow of the CRISPR/Cas9 screening. (*B*) CRISPR/Cas9 screening results in HCT116 and POP92. Stars denote the m^{6}A regulators. (*C*) The distribution of CRISPR-based dependency score of 212 common core essential genes, 781 nonessential genes, and METTL3 across 27 CRC cell lines. (*D*) CRISPR/Cas9-mediated silencing of METTL3 suppressed CRC cell colony formation. Error bars represent mean ± standard deviation from 3 independent experiments. (*E*) METTL3 mRNA expressions in paired CRC tumors and adjacent normal tissues from our CRC cohort (cohort 1, n = 127) and TCGA cohort (cohort 2, n = 50). In cohort I, the relative mRNA levels of METTL3 were normalized against β-actin. (*F*) METTL3 protein expression levels in 12 pairs of CRCs (cohort 1). The relative protein levels of METTL3 were normalized against β-actin. (*G*) Top panel: high METTL3 protein expression in cohort 3 predicted poor overall survival of patients with CRC. Bottom panel: high METTL3 mRNA expression in cohort 4 predicted worse disease-specific survival. *$P < .05$, **$P < .01$, ***$P < .001$; 2 tailed *t* test (*D*), Wilcoxon matched-pairs test (*E* and *F*), or log rank test (*G*). FDA, US Food and Drug Administration

methyltransferase, emerged as the top hit (Figure 1*B*). Additional analysis based on the CERES score data set (Avana public 18Q3) showed that METTL3 is a common essential gene in 27 CRC cell lines (Figure 1*C*). Consistently, silencing METTL3 significantly inhibited CRC cell colony formation in CRC cell lines (Figure 1*D*).

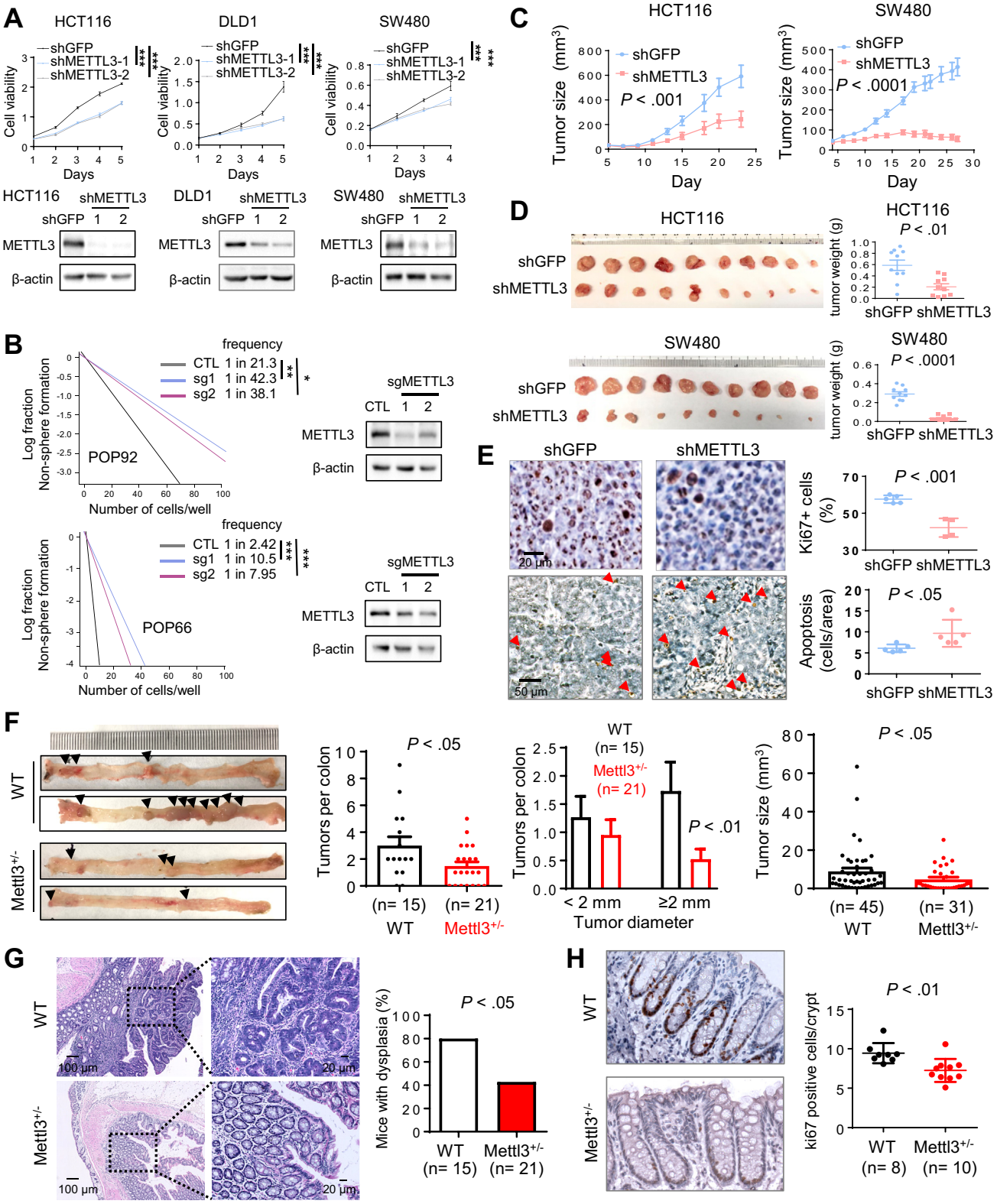

High METTL3 Expression Is Associated With Poor Prognosis in Patients With Colorectal Cancer

To assess the clinical significance of METTL3 in CRC, we examined METTL3 expression in 4 independent CRC cohorts. METTL3 mRNA expression was up-regulated in 62.2% (79/127, $P = .0027$) of CRC tumor tissues compared to paired adjacent normal tissues in our CRC cohort (cohort 1) by qPCR and in 88.0% (44/50, $P < .0001$) of CRCs from the TCGA cohort (cohort 2) (Figure 1*E*). Consistent with this, METTL3 protein was overexpressed in primary CRC tumors by Western blot (n = 12, $P = .0034$) (Figure 1*F*) and immunohistochemistry (IHC) (n = 16, $P = .0020$) (Supplementary Figure 1*A*). A positive correlation between METTL3 protein and mRNA expression was observed (n = 18, $P = .0356$) (Supplementary Figure 1*B*). We further evaluated METTL3 mRNA expression among different CRC subtypes in the TCGA cohort. Higher METTL3 expression was found in microsatellite-instability (MSI) CRC as compared to microsatellite-stable CRC (*C*Supplementary Figure 1). Consistently, among CRC consensus molecular subtypes (CMS) 1–4),[14] CMS1 (MSI enriched) showed the highest METTL3 expression (Supplementary Figure 1*C*). To investigate whether METTL3 could serve as a prognostic factor for patients with CRC, METTL3 protein expression was evaluated in a tissue microarray cohort consisting of 197 CRC cases (cohort 3) (Supplementary Figure 1*D*). High METTL3 protein expression (IHC score, 3; 35.5%, 70/197) was associated with poor overall survival ($P = .0077$) for patients with CRC (Figure 1*G*). Multivariate Cox regression analysis was carried out to assess the importance of METTL3 expression for CRC prognosis together with other risk factors including age, sex, tumor site, tumor size, and TNM stage. The result showed that high METTL3 protein expression was an independent prognostic factor for CRC (hazard ratio [HR], 1.563; 95% confidence interval [CI], 1.028–2.377; $P = .037$) (Figure 1*G*). The prognostic value of METTL3 was further validated in cohort 4, where high METTL3 mRNA expression (38.4%, 68/177) was associated with worse disease-specific survival (HR, 2.238; 95% CI, 1.272–3.936; $P = .005$) (Figure 1*G*) and overall survival (HR, 1.796; 95% CI, 1.107–2.913; $P = .018$) (Supplementary Figure 1*E*). In both cohorts, METTL3 expression did not significantly differ across TNM stages (Supplementary Figure 1*F*). Indeed, METTL3 up-regulation is evident in adenoma (Supplementary Figure 1*G*), implying that aberrant METTL3 expression is an early event in tumorigenesis. Taken together, METTL3 could serve as an independent prognostic factor for patients with CRC.

Mettl3 Knockout Inhibits Colorectal Tumorigenesis

To confirm whether METTL3 is an oncogenic factor in CRC, we silenced METTL3 in CRC cell lines using independent METTL3 short hairpin RNAs (shRNAs) in HCT116, DLD1, and SW480 cells with high METTL3 protein expression (Figure 2*A* and Supplementary Figure 2*A*), and we observed reduced CRC cell proliferation (Figure 2*A*) and colony formation (Supplementary Figure 2*B*). METTL3 knockdown induced G1-phase cell cycle arrest (Supplementary Figure 2*C*) and cell apoptosis (Supplementary Figure 2*D*). In addition, silencing of METTL3 significantly impaired the growth, sphere formation, and self-renewal capacity of colon cancer–initiating cells in POP66 and POP92 (Figure 2*B* and Supplementary Figure 2*E* and *F*). Consistently, knockdown of METTL3 markedly reduced the tumor volume and weight of HCT116, SW480, and DLD1 xenografts (Figure 2*C* and *D* and Supplementary Figure 2*G* and 2*H*). Moreover, knockdown of METTL3 inhibited cell proliferation and induced apoptosis in tumor xenografts, as shown by Ki-67 and terminal deoxynucleotidyl transferase–mediated deoxyuridine triphosphate nick-end labeling (TUNEL) staining, respectively (Figure 2*E*). Thus, METTL3 plays an oncogenic role in CRC.

To determine the role of METTL3 in colorectal tumorigenesis, we generated *Mettl3*-knockout mice (Supplementary Figure 3*A*). Because the homozygous knockout of *Mettl3* was embryonic lethal, *Mettl3* heterozygous knockout mice ($Mettl3^{+/-}$) and their wild-type (WT) littermates were treated with AOM plus DSS to induce colorectal tumors (Supplementary Figure 3*B*–*E*). As expected, $Mettl3^{+/-}$ mice had significantly fewer tumors ($P = .0303$), especially those with large size (≥2 mm, $P = .007$); reduced tumor size ($P = .0124$); and significantly less histologic dysplasia (42.8%) compared to their WT littermates (80.0%) (Figure 2*F* and *G*). Consistently, the number of $Ki67^{+}$ cells per crypt in the colon of $Mettl3^{+/-}$ mice was significantly decreased ($P = .0043$) compared with WT mice (Figure 2*H*), suggesting that silencing of METTL3 restricted the proliferation of crypt cells in carcinogen-induced colorectal tumor. We further investigated whether targeting of

Figure 2. Silencing of METTL3 inhibits colorectal tumor. (*A*) Knockdown of METTL3 significantly reduced CRC cell viability (A570). Error bars represent mean ± standard deviation from 5 independent experiments. (*B*) POP66 and POP92 were infected with CTL or specific METTL3-sgRNA lentivirus and seeded at 1, 5, 20, and 100 cells per well for 12 days. Pairwise tests for differences in stem cell frequencies from different groups were performed. Data are representative of 2 independent experiments. (*C*) HCT116 and SW480 xenografts expressing shMETTL3 (n = 10) showed significantly stunted growth compared to controls (n = 10). (*D*) Images of HCT116 and SW480 xenografts tumors. (*E*) Representative images of Ki67-positive and TUNEL-positive cells and quantitative data analysis. At least 5 fields per slide and 3 slides per animal were counted at 200× magnification. (*F*) Images of colon, tumor number, and size in littermate WT (n = 15) and $Mettl3^{+/-}$ (n = 21) mice treated with AOM-DSS. (*G*) H&E staining of colon tumors in littermate WT and $Mettl3^{+/-}$ mice. The percentages of mice with dysplasia are shown. (*H*) Ki67 staining of colon tissues in littermate WT (n = 8) and $Mettl3^{+/-}$ (n = 10) mice. Error bars in *F* represent mean ± standard error of mean. $^{*}P < .05$, $^{**}P < .01$, $^{***}P < .001$; analysis of variance test (ANOVA) (*A* and *C*), 2-tailed *t* test or Mann Whitney test (*D*, *E*, *F*, and *H*), or Fisher exact test (*G*).

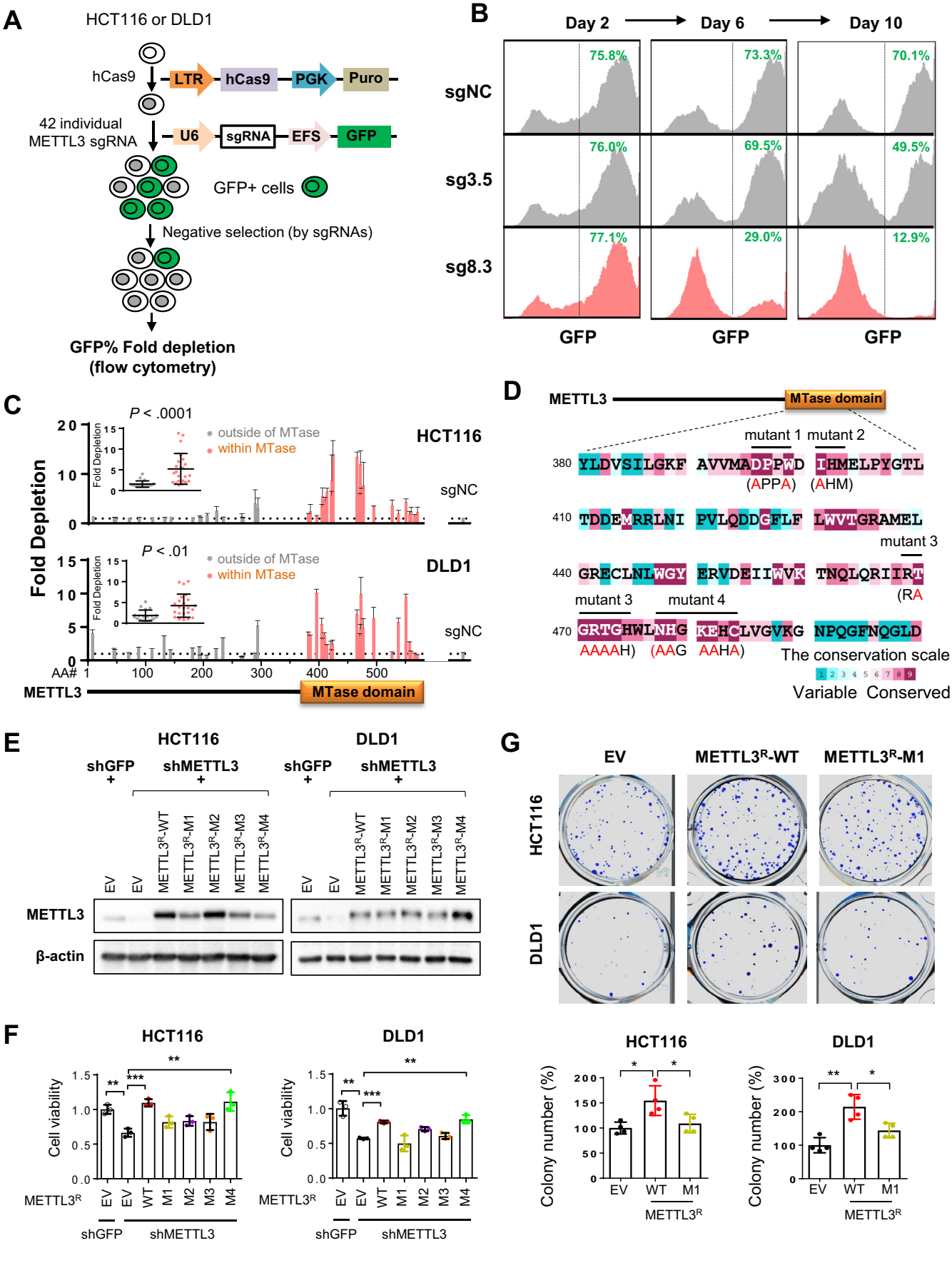
A
HCT116 or DLD1
hCas9
LTR
hCas9
PGK
Puro
42 individual METTL3 sgRNA
U6
sgRNA
EFS
GFP
GFP+ cells
Negative selection (by sgRNAs)
GFP% Fold depletion (flow cytometry)
B
Day 2
Day 6
Day 10
sgNC
sg3.5
sg8.3
75.8%
73.3%
70.1%
76.0%
69.5%
49.5%
77.1%
29.0%
12.9%
GFP
C
P < .0001
outside of MTase
within MTase
HCT116
sgNC
Fold Depletion
P < .01
DLD1
AA# 1
100
200
300
400
500
METTL3
MTase domain
D
METTL3
MTase domain
mutant 1
mutant 2
380 YLDVSILGKF AVVMADEPWD IHMELPYGTL
(APPA) (AHM)
410 TDDEMRRLNI PVLQDDGFLF LWVTGRAMEL
mutant 3
440 GRECLNLWGY ERVDEIIWVK TNQLQRIIRT
(RA
mutant 3
mutant 4
470 GRTGHWLNHG KEHCLVGVKG NPQGFNQGLD
AAAAH) (AAG AAHA)
The conservation scale
Variable Conserved
E
HCT116
DLD1
shGFP
shMETTL3
EV
METTL3R-WT
METTL3R-M1
METTL3R-M2
METTL3R-M3
METTL3R-M4
METTL3
β-actin
F
HCT116
DLD1
Cell viability
METTL3R
shGFP
shMETTL3
G
EV
METTL3R-WT
METTL3R-M1
HCT116
DLD1
Colony number (%)
METTL3R

METTL3 can inhibit colorectal tumor in a spontaneous mouse model of colon cancer by crossing *Mettl3*$^{+/-}$ mice with *Apc*$^{Min/+}$ mice (Supplementary Figure 3*F* and *G*). We found that *Apc*$^{Min/+}$*Mettl3*$^{+/-}$ mice had significantly less histologic dysplasia (5%) than *Apc*$^{Min/+}$ mice (30.4%) (Supplementary Figure 3*H*). All of these data suggest that targeting METTL3 inhibits colorectal tumorigenesis.

METTL3 Methyltransferase Domain Is Essential for Colorectal Cancer Growth

To determine the functional domains of METTL3 in colorectal tumorigenesis, we applied a domain-focused CRISPR/Cas9 approach.[15] A total of 42 sgRNAs covering all exons of METTL3 were tested, and the percentages of green fluorescent protein (GFP)$^+$ cells were tracked over time to indicate negative-selection phenotypes caused by sgRNAs (Figure 3*A*). In general, CRC cells infected with sgRNAs targeting the methyltransferase (MTase) domain were more sensitive to negative selection ($P < .0001$ and $P = .0015$ in HCT116 and DLD1, respectively) compared to those targeting outside of the MTase region (Figure 3*B* and *C*). In HCT116 and DLD1 cells, sgRNAs targeting the MTase region achieved an average of 5.22- and 4.24-fold depletion, respectively; in contrast, sgRNAs targeting outside of the MTase domain caused only minor negative-selection phenotypes (1.56- and 1.86-fold depletion in HCT116 and DLD1, respectively) (Figure 3*C*). In both cell lines, negative control sgRNA had a negligible effect (Figure 3*C*). We quantified the insertion/deletion mutations at the corresponding sgRNA cut sites by the Tracking of Indels by Decomposition (TIDE) method,[16] and equivalent genome editing efficiency among randomly selected sgRNAs was shown (Supplementary Figure 4). The MTase domain of METTL3 is thus crucial for CRC growth.

By comparing amino acid sequences of the METTL3 MTase domain across different species,[17] we located highly conserved residues within amino acids 380–500 of METTL3 (Figure 3*D*). We hypothesized that certain specific residues within the MTase domain may be vital for METTL3 function. To test this, we constructed 4 different alanine-substituted METTL3 mutants that were resistant to shMETTL3 (Figure 3*D*). WT or mutant (mut) METTL3 (mut1–4) was re-expressed in HCT116 and DLD1 cells with endogenous METTL3 depleted (Figure 3*E*). Notably, only METTL3-wt and METTL3-mut4 restored cell growth (Figure 3*F*), implying that conserved motifs 1–3 (DPPW, IHM, and RTGRTGH) were important for METTL3 function in CRC. Among these 3 motifs, DPPW was reported to be required for the catalytic activity of METTL3.[4,18] Accordingly, ectopic expression of METTL3-wt, but not METTL3-mut1, promoted colony formation in CRC cells (Figure 3*G*), corroborating that m^{6}A methyltransferase activity of METTL3 is essential for CRC growth.

METTL3 Mediates N^6-Methyladenosine Messenger RNA Methylation in Colorectal Cancer

To study whether and how METTL3 regulates m^{6}A mRNA methylation in CRC, we examined METTL3 expression and global mRNA m^{6}A level. METTL3 mRNA expression was positively correlated with m^{6}A levels (Figure 4*A*). In addition, METTL3 knockdown decreased the m^{6}A content of mRNAs in CRC (Supplementary Figure 5*A*). To comprehensively profile genes with m^{6}A modification mediated by METTL3, we performed m^{6}A-seq in HCT116 and DLD1 cells with or without METTL3 knockdown (Figure 4*B*). In total, we detected 8576; 7600; 11,018; and 9239 m^{6}A peaks, representing 3642, 3369, 3373, and 2854 transcripts in HCT116-shGFP, HCT116-shMETTL3, DLD1-shGFP, and DLD1-shMETTL3 cells, respectively (Figure 4*C*). The m^{6}A consensus motif GGAC was enriched in the detected peaks (Figure 4*C*), consistent with previous findings.[1] A similar pattern of m^{6}A distribution was observed that these m^{6}A peaks were enriched in coding sequence and 3′ UTR with a sharp density peak surrounding the stop codon (Figure 4*C*). METTL3 knockdown led to reduced number of m^{6}A peaks (Figure 4*C*) and m^{6}A abundance of common peaks (Figure 4*D*). Next, we analyzed the differential m^{6}A peaks (ratio of normalized m^{6}A read density [shGFP/shMETTL3], $\geq$2) and their corresponding transcripts by comparing the m^{6}A-seq data in CRC cells with and without shMETTL3. We identified 636 and 480 transcripts displaying reduced m^{6}A peaks by shMETTL3 in HCT116 and DLD1 cells, respectively (Figure 4*E*). Overlapping of these 2 data sets unveiled 146 common transcripts as the potential target genes of METTL3 (Figure 4*E* and Supplementary Tables 4 and 5). Several candidate genes were shown in Figure 4*F*. MeRIP-qPCR confirmed that m^{6}A modification of GLUT1 (SLC2A1), JUN, LAMC2, NUAK1, and PTTG1IP were reduced after METTL3 knockdown (Figure 4*G*). These data collectively indicate that METTL3 mediates m^{6}A mRNA methylation in CRC.

GLUT1 Is a Critical Downstream Target of METTL3

To uncover the functional downstream effectors and signaling pathways perturbed by METTL3-mediated m^{6}A

Figure 3. The methyltransferase domain of METTL3 is indispensable for CRC growth. (*A*) Flow chart of CRISPR domain–targeting screening. (*B*) Time course experiments of CRISPR domain–targeting assays evaluating sgRNAs targeting within (sg3.5) or outside of (sg8.3) the MTase domain of METTL3. (*C*) Systematic evaluation of 42 METTL3 sgRNAs. The target site of each sgRNA relative to the METTL3 protein is indicated along *x*-axis. (*D*) Evolutionary conservation of the MTase region of the METTL3 protein. Construction of mutant METTL3 plasmids is shown. (*E*) Re-expression of WT METTL3 or mutant METTL3 in HCT116 and DLD1 expressing shMETTL3. (*F*) Viability assays of HCT116 and DLD1 cells re-expressing METTL3. The relative cell viability was recorded as the absorbance (A570) to that of the control group. (*G*) Ectopic expression of METTL3-wt, but not catalytic inactive METTL3-mut1, promoted CRC cell clone formation. Error bars in *F* and *G* represent mean ± standard deviation from at least 3 independent experiments. *$P < .05$, **$P < .01$, ***$P < .001$; 2-tailed *t* test (*C*, *F*, and *G*).

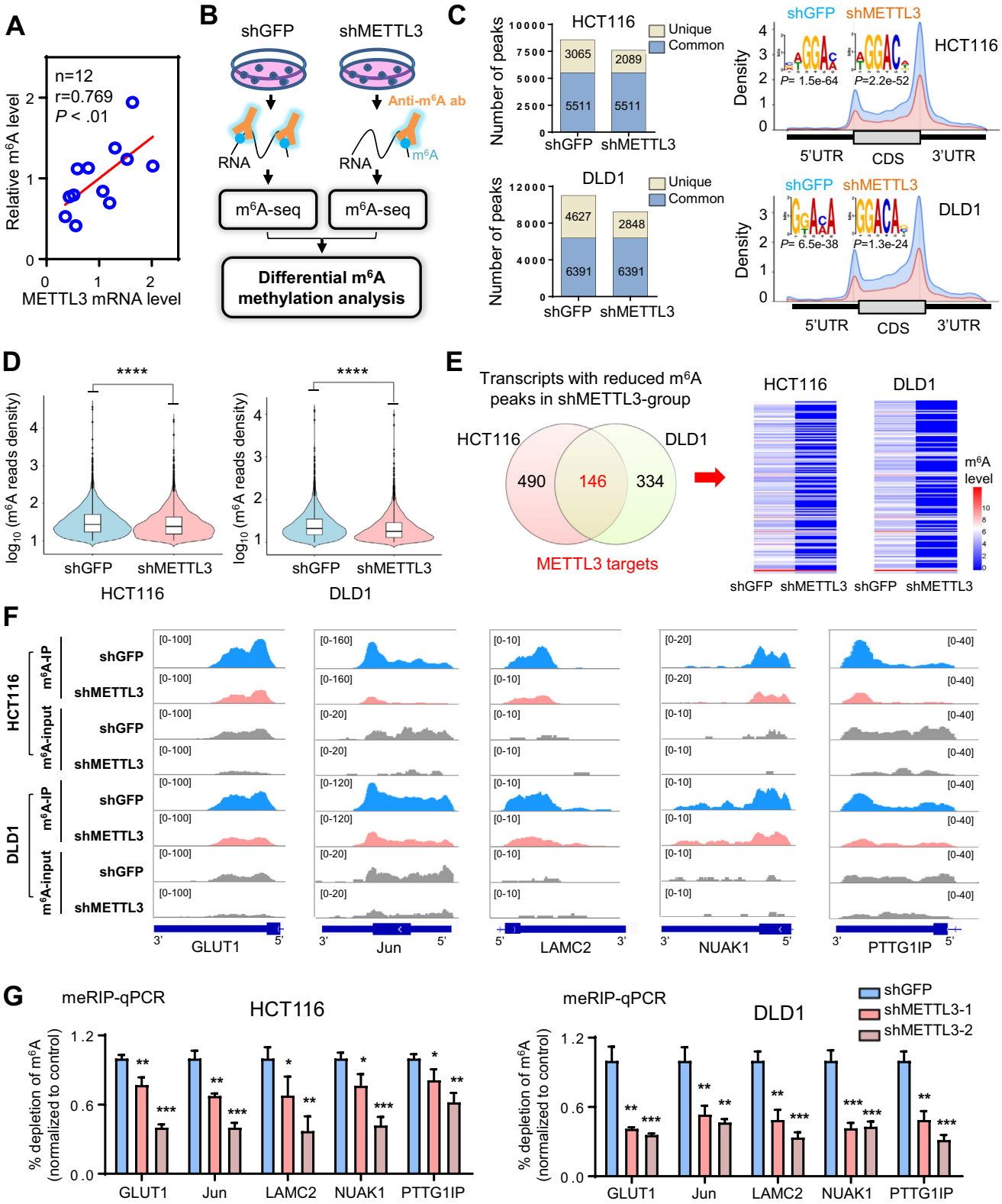

Figure 4. METTL3 catalyzes mRNA m^{6}A modification. (*A*) Correlation between METTL3 mRNA expression and global mRNA m^{6}A contents in 9 CRC and 3 normal cell lines. (*B*) Flow chart of m^{6}A-seq. (*C*) m^{6}A-seq of HCT116 and DLD1 showed a number of m^{6}A peaks. The right panel shows the normalized distribution of m^{6}A peaks and identified m^{6}A motif. (*D*) Violin plot of normalized m^{6}A reads density of common m^{6}A peaks. (*E*) Venn diagram shows overlapped transcripts with reduced m^{6}A peaks after METTL3 depletion between HCT116 and DLD1. (*F*) UCSC snapshots of m^{6}A-seq reads along indicated mRNAs. Normalized read density levels are shown as blue (shGFP), red (shMETTL3), and gray (input). Ranges of reads are indicated. (*G*) MeRIP-qPCR analysis of m^{6}A level in the select mRNAs. Results are representative of 2 independent experiments with 3 technical replicates per experiment. *$P < .05$, **$P < .01$, ***$P < .001$; Pearson *r* (*A*) or 2-tailed *t* test or Mann Whitney test (*D* and *G*). CDS, coding sequence.

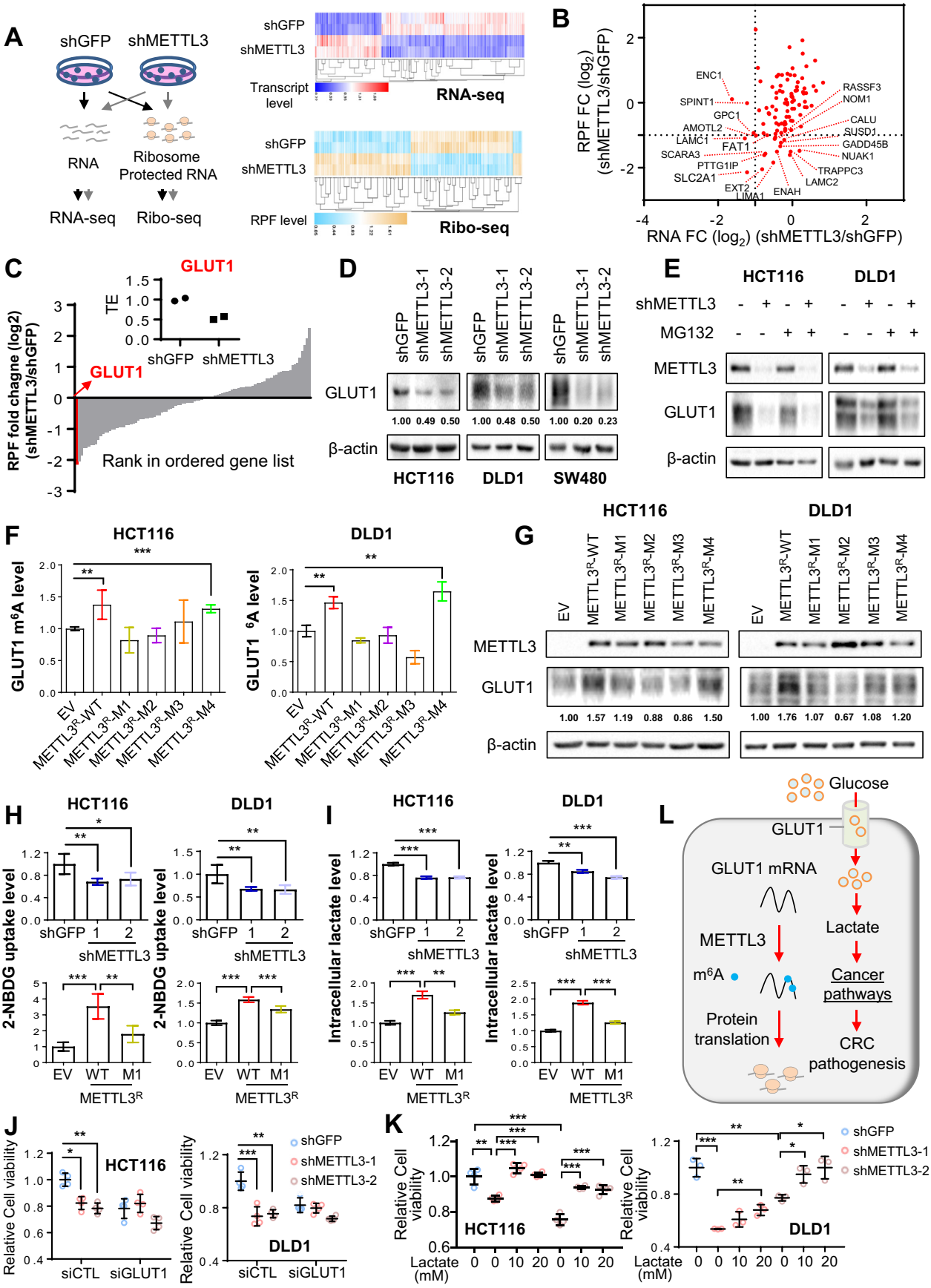
A
shGFP
shMETTL3
RNA
Ribosome Protected RNA
RNA-seq
Ribo-seq
Transcript level
RPF level
RNA-seq
Ribo-seq
B
RPF FC (log2) (shMETTL3/shGFP)
RNA FC (log2) (shMETTL3/shGFP)
ENC1
SPINT1
GPC1
AMOTL2
LAMC1
FAT1
SCARA3
PTTG1IP
SLC2A1
EXT2
LIMA1
ENAH
LAMC2
TRAPPC3
NUAK1
GADD45B
SUSD1
CALU
NOM1
RASSF3
C
GLUT1
TE
RPF fold chagne (log2) (shMETTL3/shGFP)
Rank in ordered gene list
D
shGFP
shMETTL3-1
shMETTL3-2
GLUT1
β-actin
1.00 0.49 0.50
1.00 0.48 0.50
1.00 0.20 0.23
HCT116
DLD1
SW480
E
HCT116
DLD1
shMETTL3
MG132
METTL3
GLUT1
β-actin
F
HCT116
DLD1
GLUT1 m6A level
EV
METTL3R-WT
METTL3R-M1
METTL3R-M2
METTL3R-M3
METTL3R-M4
G
HCT116
DLD1
METTL3
GLUT1
β-actin
1.00 1.57 1.19 0.88 0.86 1.50
1.00 1.76 1.07 0.67 1.08 1.20
H
HCT116
DLD1
2-NBDG uptake level
shGFP
shMETTL3
EV
WT
M1
METTL3R
I
HCT116
DLD1
Intracellular lactate level
L
Glucose
GLUT1
GLUT1 mRNA
METTL3
m6A
Protein translation
Lactate
Cancer pathways
CRC pathogenesis
J
HCT116
DLD1
Relative Cell viability
siCTL
siGLUT1
shGFP
shMETTL3-1
shMETTL3-2
K
HCT116
DLD1
Relative Cell viability
Lactate (mM)

modification, RNA-seq and Ribo-seq were performed in HCT116-shGFP and HCT116-shMETTL3 cells (Figure 5*A*). METTL3 depletion profoundly alters the gene transcriptional expression and ribosome protected fragment (RPF) abundance (Figure 5*A*). From RNA-seq, we detected 143 down-regulated and 140 up-regulated transcripts in HCT116 upon METTL3 depletion ($P < .05$; $|\log_2$ fold change$| > 1$) (Supplementary Table 6). From Ribo-Seq, 58 down-regulated and 49 up-regulated transcripts were identified after METTL3 knockdown (false discovery rate, <0.1; $|\log_2$ fold change$| > 1$) (Supplementary Table 7). Among 146 common METTL3 targets identified by m^{6}A-seq, GLUT1 was the top down-regulated gene in response to shMETTL3 (Figures 5*B* and *C*). METTL3 knockdown inhibited the translational efficiency of GLUT1 (Figure 5*C*). Concordantly, METTL3 knockdown reduced GLUT1 protein expression in HCT116, DLD1, and SW480 cells (Figure 5*D*) without affecting its mRNA abundance (Supplementary Figure 5*B*). Furthermore, proteasome inhibition using MG132 failed to restore GLUT1 protein expression in CRC cells with METTL3 silencing (Figure 5*E*), indicating that METTL3-induced GLUT1 expression does not involve alterations in protein degradation. In support of this, a significant positive correlation was observed between METTL3 and GLUT1 protein levels, but not their mRNA expression in CRC from the TCGA cohort (Supplementary Figure 5*C*).[9,19] Hence, GLUT1 is a downstream target of METTL3 in CRC.

We hypothesize that translational regulation of GLUT1 by METTL3 is m^{6}A dependent. To test this, we overexpressed METTL3-wt or METTL3 mutants in HCT116 and DLD1 cells expressing shMETTL3. Neither METTL3-wt nor METTL3-mut influenced GLUT1 mRNA levels (Supplementary Figure 5*D*). On the other hand, METTL3-wt and METTL3-mut4 increased GLUT1 m^{6}A abundance (Figure 5*F*) and protein expression (Figure 5*G*). However, mutations in conserved motifs abrogated the rescue effect of METTL3 on GLUT1 protein expression, inferring that METTL3 promotes GLUT1 protein expression in an m^{6}A-dependent manner (Figure 5*F* and *G*).

GLUT1, a facilitative glucose transporter, is frequently overexpressed in tumors and enhances glucose metabolism. Knockdown of METTL3 significantly reduced glucose uptake (Figure 5*H*) and lactate generation (Figure 5*I*). On the contrary, ectopic expression of METTL3-wt, but not the catalytically inactive METTL3, increased glucose uptake and lactate production (Figure 5*H* and *I*). We also examined the effect of METTL3 on other glucose transporters, and the results showed that knockdown of METTL3 exhibited minor effects on GLUT2, GLUT3, and GLUT4 protein expression (Supplementary Figure 5*E*). We next tested whether METTL3 promotes CRC via up-regulation of GLUT1 and glucose metabolism. Indeed, in GLUT1-deficient CRC cells, the effect of shMETTL3 on CRC cell viability was abolished (Figure 5*J*). Furthermore, treatment with lactate could rescue shMETTL3-induced suppression of cell proliferation (Figure 5*K*). All of these results suggest that METTL3 promotes GLUT1-mediated glucose metabolism in an m^{6}A-dependent manner, thereby contributing to CRC tumorigenesis (Figure 5*L*).

METTL3 Activates mTORC1 Signaling in Colorectal Cancer

To identify signaling pathways perturbed by METTL3, we performed gene set enrichment analysis of RNA-seq and Ribo-seq data, leading to the identification of 7 and 10 cancer-associated pathways, respectively (Supplementary Figure 6*A* and *B*). Remarkably, mTORC1 (mammalian target of rapamycin complex 1) signaling was identified as the common enriched gene set (Figure 6*A*) that could transduce the metabolic effects of glucose in cancer. Depletion of METTL3 was significantly associated with the inactivation of mTORC1 signaling by gene set enrichment analysis of RNA-seq and Ribo-seq data sets (Figure 6*B*). In line with these findings, a positive correlation between METTL3 expression and mTORC1 signaling was observed in the TCGA-CRC data set (Figure 6*B*).

We sought to further validate the correlation between METTL3 and mTORC1 signaling in CRC. MTOR is also an essential gene in our CRISPR/Cas9 screening. Genes having similar essentiality patterns across diverse cell lines are likely to form a functional gene network.[20] This prompted us to construct a network of genes that were coessential with METTL3 using the CERES score data set. METTL14 and mTORC1 subunits (MTOR, RPTOR, and TELO2) were among top co-correlation genes with METTL3 in CRC (Supplementary Figure 6*C* and *D*). METTL3 and METTL14 formed a stable heterodimer complex to catalyze m^{6}A modification,[21] which is reflected in their close correlation in most cancer types (Supplementary Figure 6*E*). Moreover,

Figure 5. METTL3 promotes GLUT1 translation and glucose metabolism. (*A*) Flow chart of RNA-seq and Ribo-seq. Heatmaps of transcript level (RNA-seq) and RPF abundance (Ribo-seq) are shown in the right panel. (*B*) The *x*- and *y*-axes indicate fold changes of transcript level (RNA-seq) and RPF abundance (Ribo-seq) of METTL3 targets, respectively. (*C*) Rank in the ordered gene list of METTL3 targets using RPF fold changes ($\log_2$, shMETTL3/shGFP). Top panel shows the translational efficiency (TE) of GLUT1. (*D*) shMETTL3 reduced GLUT1 protein expression. (*E*) CRC cells were treated with 10 μmol/L MG132 for 12 hours. (*F*) MeRIP-qPCR analysis of GLUT1 m^{6}A level in CRC cells re-expressing METTL3. (*G*) Western blot analysis of GLUT1 protein expression. (*H*) Glucose uptake measurement in CRC cells. (*I*) Lactate levels in CRC cells. (*J*) Proliferation assays of CRC cells infected with indicated shRNA and siRNA. The cell viability was normalized to the control groups. (*K*) CRC cells were treated with sodium lactate. The cell viability was normalized to the untreated control groups. (*L*) Up-regulation of METTL3 in CRC could increase global m^{6}A modification and promote GLUT1 protein translation and glucose metabolism, thus contributing to CRC pathogenesis. For *D*, *E*, and *G*, data are representative of 2 independent experiments. Error bars in *F* and *H–K* represent mean ± standard deviation from at least 3 independent experiments. *$P < .05$, **$P < .01$, ***$P < .001$; 2-tailed *t* test (*F* and *H–K*). FC, fold change; M, mol/L; si, small interfering.

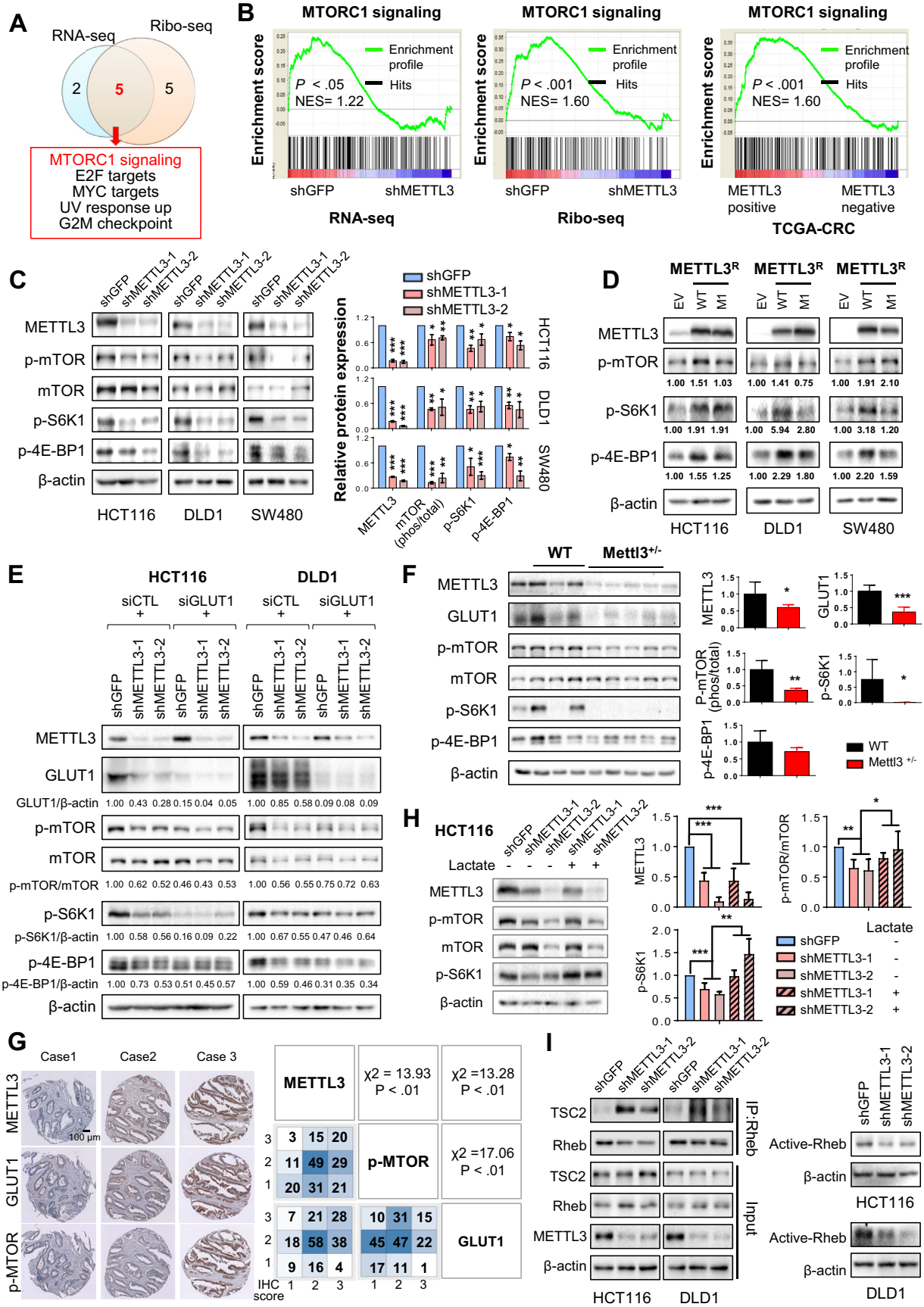
A
RNA-seq
Ribo-seq
2
5
5
MTORC1 signaling
E2F targets
MYC targets
UV response up
G2M checkpoint
B
MTORC1 signaling
Enrichment score
Enrichment profile
Hits
P < .05
NES= 1.22
shGFP
shMETTL3
RNA-seq
MTORC1 signaling
P < .001
NES= 1.60
Ribo-seq
MTORC1 signaling
P < .001
NES= 1.60
METTL3 positive
METTL3 negative
TCGA-CRC
C
shGFP
shMETTL3-1
shMETTL3-2
METTL3
p-mTOR
mTOR
p-S6K1
p-4E-BP1
β-actin
HCT116
DLD1
SW480
Relative protein expression
METTL3
mTOR (phos/total)
p-S6K1
p-4E-BP1
D
METTL3R
EV
WT
M1
METTL3
p-mTOR
1.00 1.51 1.03
1.00 1.41 0.75
1.00 1.91 2.10
p-S6K1
1.00 1.91 1.91
1.00 5.94 2.80
1.00 3.18 1.20
p-4E-BP1
1.00 1.55 1.25
1.00 2.29 1.80
1.00 2.20 1.59
β-actin
HCT116
DLD1
SW480
E
HCT116
DLD1
siCTL
siGLUT1
shGFP
shMETTL3-1
shMETTL3-2
METTL3
GLUT1
GLUT1/β-actin 1.00 0.43 0.28 0.15 0.04 0.05 1.00 0.85 0.58 0.09 0.08 0.09
p-mTOR
mTOR
p-mTOR/mTOR 1.00 0.62 0.52 0.46 0.43 0.53 1.00 0.56 0.55 0.75 0.72 0.63
p-S6K1
p-S6K1/β-actin 1.00 0.58 0.56 0.16 0.09 0.22 1.00 0.67 0.55 0.47 0.46 0.64
p-4E-BP1
p-4E-BP1/β-actin 1.00 0.73 0.53 0.51 0.45 0.57 1.00 0.59 0.46 0.31 0.35 0.34
β-actin
F
WT
Mettl3+/-
METTL3
GLUT1
p-mTOR
mTOR
p-S6K1
p-4E-BP1
β-actin
P-mTOR (phos/total)
WT
Mettl3 +/-
H
HCT116
Lactate
shGFP
shMETTL3-1
shMETTL3-2
METTL3
p-mTOR
mTOR
p-S6K1
β-actin
p-mTOR/mTOR
Lactate
G
Case1
Case2
Case 3
METTL3
GLUT1
p-MTOR
100 μm
METTL3
χ2 = 13.93
P < .01
χ2 =13.28
P < .01
p-MTOR
χ2 =17.06
P < .01
GLUT1
IHC score
I
shGFP
shMETTL3-1
shMETTL3-2
TSC2
Rheb
IP:Rheb
TSC2
Rheb
METTL3
β-actin
Input
HCT116
DLD1
Active-Rheb
β-actin
HCT116
Active-Rheb
β-actin
DLD1

we observed a CRC-biased relationship between dependency scores of METTL3 and mTORC1 subunits (Supplementary Figure 6*E*), implying a unique molecular association between m^{6}A modification and mTORC1 signaling in CRC.

We next dissected the role of METTL3 on mTORC1 signaling in CRC. Knockdown of METTL3 inactivated the mTORC1 pathway, as evidenced by reduced phosphorylation of mTOR, ribosomal protein S6 kinase beta-1 (S6K1), and eukaryotic translation initiation factor 4E-binding proteins 1 (4E-BP1) (Figure 6*C*). Translation of transcripts containing 5′ terminal oligopyrimidine tract motifs is specifically recognized by mTORC1.[22,23] We examined the translational efficiency of individual mRNAs, defined as RPF level divided by transcript level.[24] METTL3 depletion was found to reduce the translational efficiency of known terminal oligopyrimidine tract mRNAs (Supplementary Figure 7*A*), an observation that was further confirmed by analysis of published polysome profiling data sets (Supplementary Figure 7*A*).[25] Thus, targeting of METTL3 could suppress mTORC1 signaling in CRC. Furthermore, re-expression of METTL3-wt, but not catalytic inactive METTL3-mut1, promoted p-mTOR, p-S6K1, and p-4E-BP1 expression in CRC cells with depletion of endogenous METTL3 (Figure 6*D*), suggesting that METTL3-mediated m^{6}A deposition regulates mTORC1 signaling in CRC.

METTL3 Promotes the m^{6}A-GLUT1-mTORC1 Axis in Colorectal Cancer

We then investigated if GLUT1 is involved in METTL3-mediated activation of mTORC1. Knockdown of GLUT1 attenuated mTORC1 signaling cascade, including p-mTOR, p-S6K1, and p-4E-BP1 (Figure 6*E*). On the contrary, mTORC1 inhibition by rapamycin had no effect on the METTL3-GLUT1 axis (Supplementary Figure 7*B*). In GLUT1-deficient CRC cells, shMETTL3 was incapable of affecting mTORC1 signaling (Figure 6*E*), implying that METTL3 promotes mTORC1 signaling via GLUT1. To confirm these findings in vivo, we examined the effect of METTL3 depletion on the protein expression of GLUT1 and mTORC1 signaling cascade by Western blot in colon tissues of AOM/DSS-treated *Mettl3*$^{+/-}$ mice and *Apc*$^{Min/+}$*Mettl3*$^{+/-}$ mice (Figure 6*F* and Supplementary Figure 7*C*). Compared to control mice, *Mettl3*$^{+/-}$ mice showed down-regulation of GLUT1, p-mTOR, p-S6K1, and p-4E-BP1. Consistently, positive correlations were found between METTL3, GLUT1, and p-mTOR protein expression in 197 human CRC tissues by IHC (Figure 6*G*).

We next investigated the molecular basis of GLUT1-mediated mTORC1 signaling. Given that lactate is the major product of glycolysis, we hypothesize that lactate might link GLUT1 up-regulation to downstream signaling cascades. Lactate supplementation in METTL3-silenced cells rescued p-mTOR and p-S6K1 expression, indicative of mTORC1 activation (Figure 6*H* and Supplementary Figure 7*D*). We further examined upstream regulators of mTORC1. TSC2 is a negative regulator of mTORC1 signaling by inhibiting Rheb-GTP, an mTORC1 activator.[26] Coimmunoprecipitation assay showed that shMETTL3 promoted the interaction between TSC2 and Rheb, leading to reduced Rheb-GTP levels (Figure 6*I*). On the other hand, lactate reduced the TSC2-Rheb interaction and recused Rheb-GTP levels in shMETTL3 cells (Supplementary Figure 7*E* and *F*). Our data suggests that METTL3-driven GLUT1 expression and lactate production reduces TSC2-Rheb interaction, enhances Rheb-GTP levels, and thereby activates mTORC1 signaling.

mTORC1 Inhibition Potentiates the Anticancer Effect of METTL3 Silencing in Colorectal Cancer

mTORC1 signaling is an attractive target for CRC therapy. We hypothesized that the combination of METTL3 silencing and chemical inhibition of mTORC1 might achieve a better effect in CRC therapy. To this end, HCT116 and DLD1 cells with or without METTL3 knockdown were treated with rapamycin (Figure 7*A*). Although shMETTL3 or rapamycin individually inhibited cell proliferation, their combination showed a more significant inhibitory effect compared to either shMETTL3 ($P < .001$) or rapamycin alone ($P < .001$) (Figure 7*A* and Supplementary Figure 8*A*). Consistently, p-mTOR was more effectively blocked in response to shMETTL3 plus rapamycin (Figure 7*B*). We next evaluated the effect of temsirolimus (TEM), a water-soluble derivative of rapamycin, plus shMETTL3 in 2 human-derived primary CRC organoids. The combination of shMETTL3 plus TEM markedly repressed CRC organoid growth compared to either shMETTL3 or TEM alone (Figure 7*C* and *D*). We further validated the therapeutic potential of shMETTL3 plus TEM on CRC growth in vivo. The nude mice were subcutaneously inoculated with HCT116

Figure 6. METTL3 promotes m^{6}A-GLUT1-mTORC1 axis. (*A*) Venn diagram showing overlaps between gene sets analyzed by RNA-seq and Ribo-seq. (*B*) Enrichment plots of mTORC1 signaling. Right panel shows analysis of TCGA-CRC cohort. (*C*) Depletion of METTL3 inactivated mTORC1 signaling by western blot. (*D*) Ectopic expression of METTL3-wt, but not METTL3-mut1, promoted mTORC1 signaling. (*E*) HCT116 and DLD1 cells were expressed with indicated shRNA and siRNA, and Western blot was performed. (*F*) Western blot analysis of colon tissues from littermate WT and *Mettl3*$^{+/-}$ mice treated with AOM-DSS. (*G*) Representative images of METTL3, GLUT1, and p-MTOR protein expression in CRC tissue arrays (n = 197) by IHC. Right panel shows Pearson correlation analysis between METTL3, GLUT1, and p-MTOR protein expression. (*H*) HCT116 cells were infected with METTL3-shRNAs and treated with 20 mmol/L sodium lactate for 1 hour. (*I*) Immune complexes were precipitated by anti-Rheb and immunoblotted by anti-TSC2 or anti-Rheb. Rheb-GTP was determined using the Rheb Activation Assay kit (NewEastBio). The relative expression levels of individual proteins in *C*, *D*, *E*, *F*, and *H* were normalized against β-actin, except p-MTOR, which was normalized against total mTOR. For *D*, *E*, and *I*, data are representative of 2 independent experiments. Error bars in *C* and *H* represent mean ± standard deviation from at least 3 independent experiments. *$P < .05$, **$P < .01$, ***$P < .001$; 2-tailed *t* test (*C*, *F*, and *H*) or Pearson chi-square test (*G*).

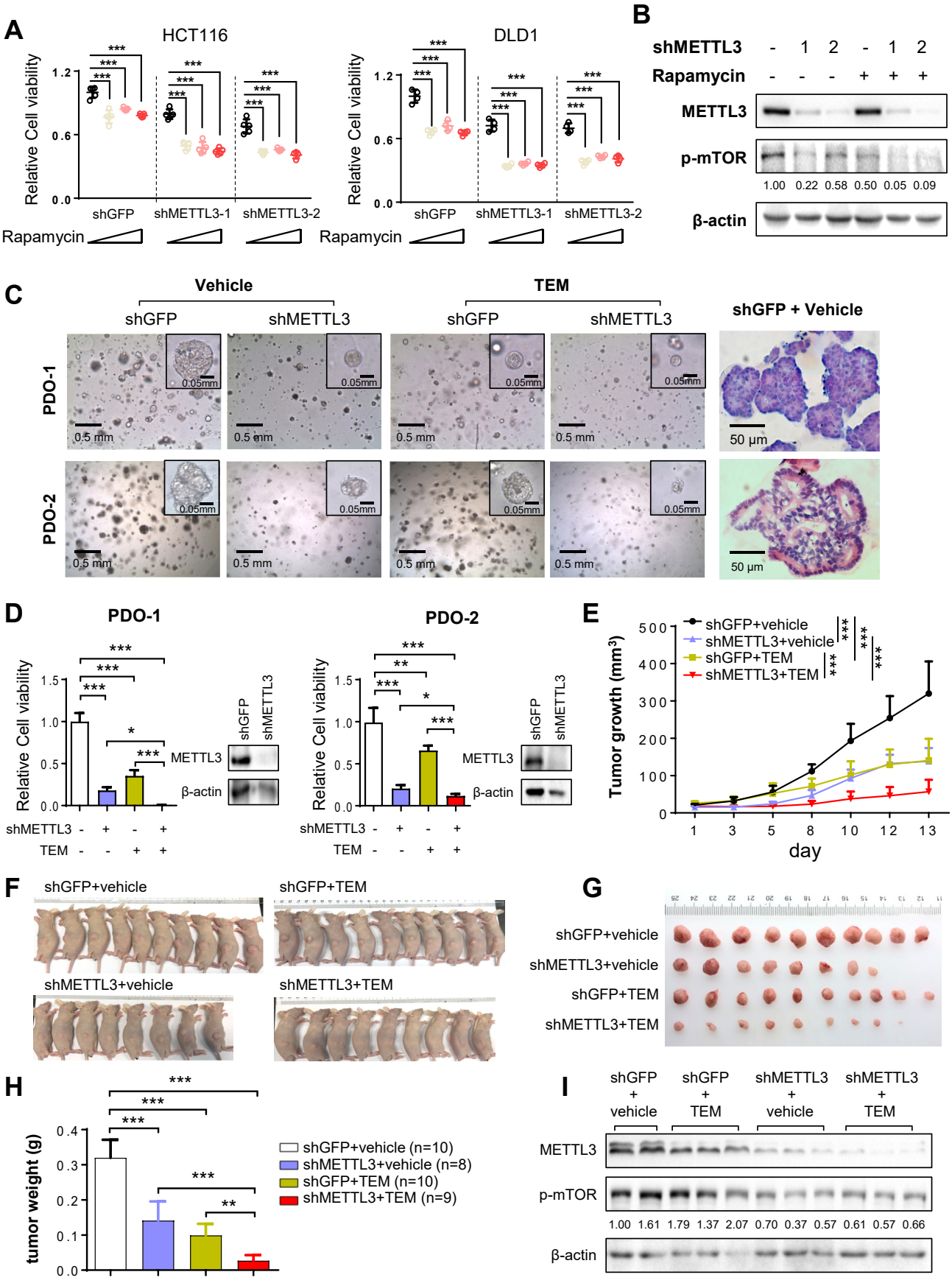
A
HCT116
DLD1
Relative Cell viability
shGFP
shMETTL3-1
shMETTL3-2
Rapamycin
B
shMETTL3 - 1 2 - 1 2
Rapamycin - - - + + +
METTL3
p-mTOR
1.00 0.22 0.58 0.50 0.05 0.09
β-actin
C
Vehicle
TEM
shGFP
shMETTL3
shGFP + Vehicle
PDO-1
PDO-2
0.5 mm
0.05mm
50 μm
D
PDO-1
PDO-2
Relative Cell viability
shMETTL3 - + - +
TEM - - + +
METTL3
β-actin
E
shGFP+vehicle
shMETTL3+vehicle
shGFP+TEM
shMETTL3+TEM
Tumor growth (mm³)
day
F
shGFP+vehicle
shGFP+TEM
shMETTL3+vehicle
shMETTL3+TEM
G
H
tumor weight (g)
shGFP+vehicle (n=10)
shMETTL3+vehicle (n=8)
shGFP+TEM (n=10)
shMETTL3+TEM (n=9)
I
shGFP + vehicle
shGFP + TEM
shMETTL3 + vehicle
shMETTL3 + TEM
METTL3
p-mTOR
1.00 1.61 1.79 1.37 2.07 0.70 0.37 0.57 0.61 0.57 0.66
β-actin

cells with or without shMETTL3, followed by intraperitoneal administration of TEM 3 times a week. Targeting METTL3 or administration of TEM alone modestly reduced tumor size and weight as compared to vehicle control (Figure 7*E*–*H*). As expected, combination treatment resulted in more significant suppression of HCT116 xenograft tumor growth (Figure 7*E*–*H*). Consistently, p-mTOR was significantly suppressed in response to shMETTL3 plus TEM (Figure 7*I*). In keeping with this, knockout of METTL3 combined with TEM treatment achieved the most significant effect in suppressing colorectal tumor using $Apc^{Min/+}$ mice model (Supplementary Figure 8*B*–*E*). Our data collectively show that mTORC1 inhibitors can potentiate the anticancer effect of METTL3 silencing in CRC.

Discussion

In this study, we systematically screened the dependencies of epigenetic regulators and US Food and Drug Administration–approved drug targets using a unique CRISPR/Cas9 library, showing that METTL3 is the most essential m^{6}A regulatory enzyme for CRC. We established the causality of METTL3 in promoting colorectal tumorigenesis and elucidated GLUT1-mTORC1 as the primary target of METTL3 in CRC. Combinatorial targeting of METTL3 and mTORC1 shows promising effects to suppress CRC growth, indicating that METTL3 is a potential therapeutic target for CRC.

METTL3 is consistently overexpressed in CRC from multiple CRC patient cohorts. Moreover, patients with high METTL3 expression in CRC had significantly worse prognosis, an observation that could be well explained by the oncogenic properties of METTL3. Silencing of METTL3 suppressed cell proliferation in CRC cells, an effect that primarily involves inhibition of cell cycle progression and induction of apoptosis. In accordance with in vitro data, silencing of METTL3 markedly suppressed colorectal tumor in a xenograft model and transgenic mouse models. Consistently, METTL3 was reported to exert oncogenic functions in glioblastoma,[3] lung cancer,[4] hepatocellular carcinoma,[27] and acute myeloid leukemia.[5,6]

METTL3 is a master regulator of m^{6}A modification. Accordingly, METTL3 ablation in CRC cell lines suppressed global m^{6}A level. METTL3 was reported to promote the translation of specific oncogenes in m^{6}A methyltransferase activity–dependent[5] and –independent manners.[4] Through domain-focused CRISPR/Cas9 screening and mutagenesis studies, the MTase domain of METTL3 was pinpointed as indispensable for CRC growth. In particular, we identified several key conserved motifs (DPPW, IHM, and RTGRTGH), whose mutations were found to abrogate the oncogenic function of METTL3. Supporting our observations, DPPW has been reported as the main catalytic motif of METTL3.[18] On the other hand, the RTGRTGH motif is located at the interface of METTL3 and METTL14[28]; mutation of RTGRTGH motif may thus interfere with the formation of METTL3-METTL14 heterodimer complex necessary for effective MTase activity. Taken together, our findings suggest that m^{6}A methyltransferase activity is essential for the oncogenic role of METTL3 in CRC.

Integrative m^{6}A-seq, RNA-seq, and Ribo-seq analysis identified GLUT1, a facilitative glucose transporter, as the top repressed gene in METTL3-knockdown cells. GLUT1 is up-regulated in a wide variety of cancers, increasing glucose uptake and subsequent glucose metabolism to support tumor cell growth and survival. METTL3 catalyzed GLUT1 m^{6}A modification to induce GLUT1 protein translation, resulting in enhanced glucose uptake and lactate generation. Critically, mutations of conserved motifs (DPPW, IHM, or RTGRTGH) in METTL3 disrupted its effect on m^{6}A modification and protein expression of GLUT1, glucose metabolism, and subsequent promotion of tumorigenesis, implying an essential role of METTL3 MTase domain in this signaling axis.

Integrative RNA-seq and Ribo-seq analysis in CRC cells identified mTORC1 signaling that was modulated by METTL3. mTORC1 is a critical signaling node that integrates nutrient sensing to coordinate biosynthesis. Hyperactivation of mTORC1 is a common molecular event in CRC.[29–31] Silencing of METTL3 attenuated the mTORC1 signaling cascade, including p-mTOR, p-S6K1, and p-4E-BP1. Moreover, METTL3 expression was positively correlated with mTORC1 activity (p-mTOR Ser2448)[32] in a CRC patient cohort (n = 197), implying that METTL3 promotes mTORC1 activation in vitro and in vivo. mTORC1 activation by METTL3 depends on GLUT1-mediated glucose metabolism, because GLUT1 knockdown or lactate supplementation could abolish or reverse, respectively the inhibitory effect of shMETTL3 on mTORC1 signaling. Conversely, mTORC1 blockade in CRC cells has no effect on METTL3-mediated GLUT1 expression, indicating that METTL3 promoted GLUT1 translation independently of mTORC1. Collectively, our study identifies, to our knowledge, a novel METTL3-m^{6}A-GLUT1-mTORC1 axis central to the protumorigenic effect of METTL3 in CRC.

Targeting mTORC1 signaling by rapamycin and rapalogs has been proposed as a potential approach for cancer therapy. However, application of mTORC1 inhibitors in CRC

Figure 7. Use of mTORC1 inhibitors combined with METTL3 silencing to suppress CRC. (*A*) Cells were treated with rapamycin for 4 days. The cell viability was normalized to the untreated control groups. (*B*) Western blot analysis of DLD1 cells treated with 10 μmol/L rapamycin for 12 hours. (*C*) Representative images of patient-derived CRC organoids treated with control vehicle or 10 μmol/L temsirolimus for 5 days. (*D*) Cell viability assays of patient-derived CRC organoids treated with control vehicle or 10 μmol/L temsirolimus for 3 days. The cell viability was normalized to the untreated control groups. (*E*) Analysis of HCT116 xenograft growth curves. (*F*) Images of mice with xenografts tumors. (*G*) Image of HCT116 xenografts upon harvesting. (*H*) Histogram of HCT116 xenograft weight. (*I*) Western blot analysis of HCT116 xenografts. For *B* and *C*, data are representative of 2 independent experiments. Error bars in *A* and *D* represent mean ± standard deviation from at least 3 independent experiments. $^*P < .05$, $^{**}P < .01$, $^{***}P < .001$; ANOVA test (*A*, *D*, *E*, and *F*).

remains limited to preclinical investigations, owing to their modest efficacy.[33] Combination approaches targeting multiple components of mTORC1 signaling might improve its efficacy for CRC. To this end, we proposed a rational combination of mTORC1 inhibition plus METTL3 depletion for treatment of CRC. Indeed, pharmacologic blockade of mTORC1 was found to facilitate the growth inhibitory effect of METTL3 depletion in CRC. One possible explanation for this phenomenon might be induction of apoptosis by METTL3 depletion, given that rapamycin and rapalogs are generally cytostatic rather than cytotoxic.[34] Another possibility is that depletion of METTL3 could suppress p-4E-BP1 (Thr37/46), which is otherwise resistant to rapamycin and rapalogs.[35] Notably, we observed that high METTL3 expression is associated with the MSI phenotype. Given that MSI status of CRC may influence the outcomes of patients treated with adjuvant chemotherapy or immunotherapy,[36] it will be of great value to further investigate the role of METTL3 in modulating chemotherapy or immunotherapy efficacy in future studies. Taken together, high METTL3 expression is a poor prognostic factor and a potential therapeutic target for patients with CRC.

Our study has some potential limitations, because we focused on the role of METTL3 in CRC cells without considering its effect on the tumor microenvironment. Emerging studies suggest that m^{6}A modification participates in both innate and adaptive immune responses.[37] We are establishing conditional *Mettl3*-knockout mouse models to further evaluate the effect of cell type–specific *Mettl3* knockout on colorectal carcinogenesis.

In conclusion, we identified that METTL3 is an essential m^{6}A regulator enzyme in colorectal carcinogenesis. METTL3 promotes CRC initiation and progression through inducing an m^{6}A-GLUT1-mTORC1 axis. High METTL3 expression is associated with poor survival of patients with CRC. Cotargeting of METTL3 and mTORC1 suppressed colorectal carcinogenesis.

Supplementary Material

Note: To access the supplementary material accompanying this article, visit the online version of *Gastroenterology* at www.gastrojournal.org, and at https://doi.org/10.1053/j.gastro.2020.11.013.

References

1. Meyer KD, Saletore Y, Zumbo P, et al. Comprehensive analysis of mRNA methylation reveals enrichment in 3′ UTRs and near stop codons. Cell 2012;149:1635–1646.
2. Zhao BS, Roundtree IA, He C. Post-transcriptional gene regulation by mRNA modifications. Nat Rev Mol Cell Biol 2017;18:31–42.
3. Visvanathan A, Patil V, Arora A, et al. Essential role of METTL3-mediated m^{6}A modification in glioma stem-like cells maintenance and radioresistance. Oncogene 2018;37:522–533.
4. **Lin S, Choe J**, Du P, et al. The m^{6}A methyltransferase METTL3 promotes translation in human cancer cells. Mol Cell 2016;62:335–345.
5. **Vu LP, Pickering BF, Cheng Y**, et al. The *N*^{6}-methyladenosine (m^{6}A)-forming enzyme METTL3 controls myeloid differentiation of normal hematopoietic and leukemia cells. Nat Med 2017;23:1369–1376.
6. **Barbieri I, Tzelepis K, Pandolfini L**, et al. Promoter-bound METTL3 maintains myeloid leukaemia by m^{6}A-dependent translation control. Nature 2017;552(7683):126–131.
7. Zhang S, Zhao BS, Zhou A, et al. m^{6}A demethylase ALKBH5 maintains tumorigenicity of glioblastoma stem-like cells by sustaining FOXM1 expression and cell proliferation program. Cancer Cell 2017;31:591–606.
8. **Huang Y, Su R, Sheng Y**, et al. Small-molecule targeting of oncogenic FTO demethylase in acute myeloid leukemia. Cancer Cell 2019;35:677–691.
9. The Cancer Genome Atlas Network. Comprehensive molecular characterization of human colon and rectal cancer. Nature 2012;487(7407):330–337.
10. **Zeng Y, Wang SY**, Gao SS, et al. Refined RIP-seq protocol for epitranscriptome analysis with low input materials. PLoS Biol 2018;16(9):e2006092.
11. Antanaviciute A, Baquero-Perez B, Watson CM, et al. m6aViewer: software for the detection, analysis, and visualization of *N*^{6}-methyladenosine peaks from m^{6}A-seq/ME-RIP sequencing data. RNA 2017;23:1493–1501.
12. Love MI, Huber W, Anders S. Moderated estimation of fold change and dispersion for RNA-seq data with DESeq2. Genome Biol 2014;15(12):550.
13. **de Klerk E, Fokkema IF, Thiadens KA**, et al. Assessing the translational landscape of myogenic differentiation by ribosome profiling. Nucleic Acids Res 2015;43:4408–4428.
14. **Guinney J, Dienstmann R, Wang X**, et al. The consensus molecular subtypes of colorectal cancer. Nat Med 2015;21:1350–1356.
15. Shi J, Wang E, Milazzo JP, et al. Discovery of cancer drug targets by CRISPR-Cas9 screening of protein domains. Nat Biotechnol 2015;33:661–667.
16. Brinkman EK, Chen T, Amendola M, et al. Easy quantitative assessment of genome editing by sequence trace decomposition. Nucleic Acids Res 2014;42(22):e168.
17. Ashkenazy H, Abadi S, Martz E, et al. ConSurf 2016: an improved methodology to estimate and visualize evolutionary conservation in macromolecules. Nucleic Acids Res 2016;44:W344–W350.
18. **Wang X, Feng J, Xue Y**, et al. Structural basis of *N*^{6}-adenosine methylation by the METTL3–METTL14 complex. Nature 2016;534(7608):575–578.
19. Zhang B, Wang J, Wang X, et al. Proteogenomic characterization of human colon and rectal cancer. Nature 2014;513(7518):382–387.
20. Wang T, Yu H, Hughes NW, et al. Gene essentiality profiling reveals gene networks and synthetic lethal interactions with oncogenic Ras. Cell 2017;168:890–903.
21. **Liu J, Yue Y**, Han D, et al. A METTL3–METTL14 complex mediates mammalian nuclear RNA *N*^{6}-adenosine methylation. Nat Chem Biol 2014;10:93–95.
22. Thoreen CC, Chantranupong L, Keys HR, et al. A unifying model for mTORC1-mediated regulation of mRNA translation. Nature 2012;485(7396):109–113.

23. **Hsieh AC, Liu Y**, Edlind MP, et al. The translational landscape of mTOR signalling steers cancer initiation and metastasis. Nature 2012;485(7396):55–61.
24. Ingolia NT, Lareau LF, Weissman JS. Ribosome profiling of mouse embryonic stem cells reveals the complexity and dynamics of mammalian proteomes. Cell 2011; 147:789–802.
25. **Choe J, Lin S**, Zhang W, et al. mRNA circularization by METTL3–eIF3h enhances translation and promotes oncogenesis. Nature 2018;561(7724):556–560.
26. **Inoki K, Li Y**, Xu T, et al. Rheb GTPase is a direct target of TSC2 GAP activity and regulates mTOR signaling. Genes Dev 2003;17:1829–1834.
27. Chen M, Wei L, Law CT, et al. RNA N6-methyladenosine methyltransferase-like 3 promotes liver cancer progression through YTHDF2-dependent posttranscriptional silencing of SOCS2. Hepatology 2018;67:2254–2270.
28. Śledź P, Jinek M. Structural insights into the molecular mechanism of the m^{6}A writer complex. Elife 2016;5: e18434.
29. Nozawa H, Watanabe T, Nagawa H. Phosphorylation of ribosomal p70 S6 kinase and rapamycin sensitivity in human colorectal cancer. Cancer Lett 2007;251:105–113.
30. Kaur H, Moreau R. Role of mTORC1 in intestinal epithelial repair and tumorigenesis. Cell Mol Life Sci 2019;76:2525–2546.
31. Prossomariti A, Piazzi G, Alquati C, et al. Are Wnt/β-catenin and PI3K/AKT/mTORC1 distinct pathways in colorectal cancer? Cell Mol Gastroenterol Hepatol 2020; 10:491–506.
32. Chiang GG, Abraham RT. Phosphorylation of mammalian target of rapamycin (mTOR) at Ser-2448 is mediated by p70S6 kinase. J Biol Chem 2005; 280:25485–25490.
33. Kim DD, Eng C. The promise of mTOR inhibitors in the treatment of colorectal cancer. Expert Opin Investig Drugs 2012;21:1775–1788.
34. Li J, Kim SG, Blenis J. Rapamycin: one drug, many effects. Cell Metab 2014;19:373–379.
35. Kang SA, Pacold ME, Cervantes CL, et al. mTORC1 phosphorylation sites encode their sensitivity to starvation and rapamycin. Science 2013;341(6144):1236566.
36. Carethers JM, Smith EJ, Behling CA, et al. Use of 5-fluorouracil and survival in patients with microsatellite-unstable colorectal cancer. Gastroenterology 2004; 126:394–401.
37. Wang YN, Yu CY, Jin HZ. RNA N^6-methyladenosine modifications and the immune response. J Immunol Res 2020;2020:6327614.

Author names in bold designate shared co-first authorship.

Received April 26, 2020. Accepted November 10, 2020.

Correspondence
Address correspondence to: Jun Yu, MD, PhD, Room 707, Li Ka Shing Medical Science Building, Prince of Wales Hospital, Shatin, New Territories, Hong Kong. e-mail: junyu@cuhk.edu.hk.

Acknowledgments
The authors thank Prof Richard I. Gregory (Boston Children's Hospital) for the gift of plasmid, Prof Jiafu Ji (Peking University Cancer Hospital), Xiaohong Wang (Peking University Cancer Hospital), Prof Anthony W.H. Chan (CUHK) and Prof Ka-Fai TO (CUHK) for the support of research using clinical samples, Minnie Y. Y. Go (CUHK), Xiang Zhang (CUHK), Ying Luo (Xiamen University) and Zeyuan Liu (Xiamen University) for the help of research using transgenic mice.

CRediT Authorship Contributions
Huarong Chen, PhD (Conceptualization: Equal; Formal analysis: Equal; Investigation: Lead; Methodology: Lead; Writing – original draft: Lead); Shanshan Gao, PhD (Investigation: Supporting; Methodology: Supporting; Validation: Supporting); Weixin Liu, Master (Formal analysis: Equal; Investigation: Supporting; Methodology: Supporting); Chi-Chun Wong, PhD (Conceptualization: Supporting; Validation: Supporting; Writing – review & editing: Equal); Jianfeng Wu, PhD (Investigation: Supporting); Jingtong Wu, Master (Investigation: Supporting); Dabin Liu, PhD (Investigation: Supporting); Hongyan Gou, PhD (Investigation: Supporting); Wei Kang, PhD (Investigation: Supporting; Resources: Supporting); Jianning Zhai, PhD (Investigation: Supporting); Chuangen Li, PhD (Investigation: Supporting); Hao Su, Master (Investigation: Supporting); Shiyan Wang, PhD (Resources: Supporting); Fraser Soares, PhD (Formal analysis: Supporting); Jiahuai Han, PhD (Resources: Supporting); Housheng Hansen He, PhD (Resources: Supporting); Jun Yu, PhD (Conceptualization: Lead; Funding acquisition: Lead; Supervision: Lead; Writing – review & editing: Lead).

Conflicts of interest
The authors disclose no conflicts.

Funding
This project was supported by National Key R&D Program of China (No. 2018YFC1315000/2018YFC1315004), National Natural Science Foundation of China (NSFC; 81972576), RGC-GRF Hong Kong (14110819, 14101917, 14108718); RGC-CRF Hong Kong (C4039-19GF, C7065-18GF), Science and Technology Program Grant Shenzhen (JCYJ20170413161534162 and JCYJ20180307151253271).

Supplementary Methods

Cell Lines and Colorectal Cancer Patient-Derived Organoid Model

The human CRC cell lines HCT116, DLD1, and SW480 were purchased from the American Type Culture Collection. The 293T cell line was purchased from Invitrogen. All cells were cultured in Dulbecco's modified Eagle medium supplemented with 10% fetal bovine serum (Thermo Fisher Scientific) and maintained at 37°C in a humidified incubator with 5% CO_2. Human cancer stem cells spheroids (POP92, POP66) and CRC patient-derived organoids were kindly provided by Prof Catherine O'Brien, Department of Surgery at University Health Network, and cultured as previously described.[1]

Targeted Clustered Regularly Interspaced Short Palindromic Repeats/Cas9 Dropout Screening

Our CRISPR/Cas9 library consists of 12,500 unique sgRNAs. The library comprises m^6A writers (METTL3, METTL14, and WTAP), readers (YTHDF1-3, YTHDC1-2, and HNRNPA2B1), and erasers (ALKBH5 and FTO). Stable Cas9-expressing CRC cell lines were generated by using the pCDH-EF1-Cas9 (NLS)-T2A-copGFP lentivirus (Cellecta) and then infected with the library at a multiplicity of infection of approximately 0.3. Cells were selected by puromycin treatment for 24–48 hours and passaged every 3–4 days before sequencing. Genomic DNA was extracted for replicate samples. The sgRNA inserts were amplified by PCR and used for library preparation. Genomic DNA was used as input, and libraries were sequenced on an Illumina HiSeq2500. The sequencing data were first aligned to the sgRNs library by bowtie, version 1.2.2.[2] The read count for each sgRNA was calculated, and the significantly enriched genes were selected by MAGeCK.[3]

Analysis of Gene Essentiality Profiling

The CERES score data set of 485 cancer cell lines (Avana public 18Q3) was downloaded from the Dependency Map (DepMap) portal (https://depmap.org/portal/). Gene pairs are ranked by Pearson correlation.

Clustered Regularly Interspaced Short Palindromic Repeats Domain–Targeting Assay

All sgRNAs in this study were designed by Massachusetts Institute of Technology CRISPR Design (http://crispr.mit.edu). To minimize off-target effects, only sgRNAs with a quality score above 70 were used in this study. Sequences of the sgRNAs targeting constitutive coding exons of METTL3 are provided in Supplementary Table 8. HCT116 or DLD1 cells were infected with LentiV_Cas9_puro (Addgene no. 108100), followed by puromycin selection to derive cells stably expressing Cas9. Cas9-expressing human cell lines were infected with sgRNA linked with GFP (LRG2.1 vector, Addgene no. 108098). The percentage of GFP-positive cells was measured every 4 days from day 2 to day 10 after infection for HCT116 and day 2 to day 14 for DLD1 by using the BD FACSCelesta flow cytometer (BD Biosciences). Final GFP and initial GFP percentages were used to calculate fold depletion. Two independent experiments were performed for each screening.

Tissue Microarray Assay

Archival formalin-fixed, paraffin-embedded tissue specimens from 208 patients with CRC who underwent colectomy at the same hospital between 1995 and 2014 were retrieved. All specimens were reviewed by an expert gastrointestinal pathologist (Prof Ka-Fai TO) to confirm histologic diagnosis and tumor cell content.[4] Clinicopathologic information was retrieved from the hospital database, last updated in December 2015. IHC[5] was performed on CRC tissue microarrays with METTL3 (1:200 dilution, Proteintech no. 15073-1-AP), GLUT1 (1:100 dilution, CST no. 12939), and p-MTOR (1:100 dilution, CST no. 2976) antibody. The staining scores of METTL3, GLUT1, and p-MTOR were determined by 2 pathologists independently (Dr Wei Kang and Prof Anthony W.H. Chan). IHC score 1: $<$10% staining; IHC score 2: $\leq$70% weak or moderate staining or strong staining in 10%–30%; IHC score 3: moderate staining in $>$70% or strong staining in $>$30%.

Lentivirus Production

HEK293T cells were used for lentivirus production. For HEK293T cells in a 10-cm dish, 8 μg of plasmid DNA, 6 μg of psPAX2 (Addgene no. 12260), 2 μg of pMD2.G (Addgene no. 12259), and 36 μL of lipofectamine 2000 (Life Tech) were mixed. Media was changed 6 hours after transfection, and the supernatant was collected at 48 and 72 hours after transfection. Two shRNAs targeting METTL3 (shMETTL3-1: 5′-CCGGGCCAAGGAACAATCCATTGTTCTCGAGAACAATGGATTGTTCCTTGGCTTTTTG-3′ and shMETTL3-2: 5′-CCGGGCAAGTATGTTCACTATGAAACTCGAGTTTCATAGTGACATACTTGCTTTTTG-3′) and a nontargeting RNA sequence serving as a negative control were purchased from Sigma-Aldrich.

Cell Viability and Colony Formation Assay

For cell viability assays, the CRC cells were first transduced with lentiviral carrying specific METTL3-shRNA. After puromycin selection for 2 days, cells (1×10^3 per well) were seeded in a 96-well plate and MTT assay (5 mg/ml; Promega) was performed accordingly.[6] For colony-formation assay, cells (500 per well) were seeded in s 12-well plate. After 2 weeks, colonies were fixed and stained with crystal violet. Proteasome inhibitor carbobenzoxy-Leu-Leu-leucinal (MG132) was purchased from Cell Signaling Technology. Rapamycin was from Sigma-Aldrich. For rescue experiments, cells were treated with 20 mmol/L sodium L-lactate (Sigma) or 20 mmol/L sodium chloride.

Small Interfering RNA–Mediated Gene Silencing

Glut1 siRNA (sc-35493) and a nontargeting RNA were used. Cells were transfected by using Lipofectamine 2000 (Invitrogen).

Cell Cycle and Apoptosis Assay

For cell cycle assay, cells were fixed in 70% ethanol and stained with propidium iodide (BD Biosciences). Apoptosis was determined using the Annexin-phycoerythrin/7-aminoactinomycin D staining kit (BD Biosciences).

Real-Time Quantitative Polymerase Chain Reaction

Total RNA was extracted from cells and tissues by using Trizol reagent (Life Tech). Complementary DNA was synthesized from total RNA by using the High-Capacity RNA-to-cDNA Kit (Life Tech). Quantitative reverse-transcription PCR was performed by using a LightCycler 480 real-time PCR system (Roche Applied Sciences) using Light-Cycler 480 SYBR Green I Master Mix (Roche) following the manufacturer's instructions. The primers used are listed in Supplementary Table 3. Gene expression was normalized to β-actin and calculated by using the $2^{-\Delta\Delta Ct}$ method.

Western Blot Analysis

Primary antibodies used are listed: Phospho-mTOR (Ser2448) (no. D9C2), mTOR (no. 2983), Phospho-p70 S6 Kinase (Thr389) (no. 108D2), Phospho-4E-BP1 (Thr37/46) (no. 236B4), Glut1 (no. 12939S), β-actin (no. 4970), and Anti-rabbit IgG (no. 7074) from Cell Signaling Technology. Protein quantification was performed by ImageJ (National Institutes of Health).

Immunoprecipitation

Immunoprecipitation assay was performed accordingly.[5] In brief, immune complexes were precipitated by anti-Rheb (Cell Signaling Technology no. 13879S) and immunoblotted by anti-TSC2 (Cell Signaling Technology no. 4308T) or anti-Rheb.

Rheb-GTP assay

Rheb-GTP expression was measured by the Rheb Activation Assay Kit (NewEast Biosciences) according to the manufacturer's instructions.

RNA N^6-Methyladenosine Quantification Assays

Total cellular mRNA was purified from total RNA by using Dynabeads Oligo (dT)25 (Thermo Fisher no. 61002) and quantified by Quant-iT RiboGreen RNA Assay Kit (Thermo Fisher no. R11490). For m^6A dot blot, equal amounts of mRNA were spotted to a nylon membrane (Thermo Fisher Scientific), followed by UV crosslinking for 10 minutes. After blocking in PBST containing 5% bovine serum albumin and 0.1% Tween-20 for 1 hour, the membrane was incubated with anti-m^6A antibody (1:1000, Abcam no. ab151230) overnight at 4°C. The membrane was incubated with horseradish peroxidase–conjugated anti-rabbit IgG (1:10,000) for 0.5 hour and visualized by using Clarity Western ECL Substrate, (GE Healthcare no. 1705061). The m^6A enzyme-linked immunosorbent assay was performed by using EpiQuik m6A RNA Methylation Quantification Kit (Epigentek no. P-9005-48) according to the protocol provided by the company.

Subcutaneous Xenograft Mouse Models

For subcutaneous xenografts, CRC cells transduced with lentiviral-carrying shCTL and shMETTL3-1 were injected subcutaneously into the left and right dorsal flanks of 4-week-old male Balb/c nude mice (2×10^6 cells in 0.1 mL phosphate-buffered saline/mouse), respectively. Tumor size was measured every 2 days with a digital caliper. Tumor volume (mm^3) was calculated as follows: volume = (shortest diameter)^2 × (longest diameter) × 0.5. At the endpoint, tumors were harvested and weighted. To investigate the synergistic effect of mTOR inhibitor and shMETTL3 on CRC growth in vivo, HCT116 (2×10^6 cells) cells were injected subcutaneously into the dorsal flanks of 4-week-old male Balb/c nude mice. Temsirolimus (Tocris Bioscience no. 5264/10) was dissolved in 100% ethanol to a stock concentration of 50 mg/ml and diluted to a final concentration of 2 mg/mL in 5% Tween 20, 5% polyethylene glycol 400, and normal saline solution. Mice were administered with temsirolimus intraperitoneally (10 mg/kg body weight) 3 times per week 5 days after HCT116 injection. Control mice were injected with vehicle. Three mice that failed to develop tumors 5 days after injection of HCT116-shMETTL3 cells were removed from the study. All animal studies were performed in accordance with the guidelines approved by the Animal Experimentation Ethics Committee of CUHK.

Pathway Analysis

Overrepresentation analysis of METTL3 target genes was performed by using the online platform WebGestalt (http://www.webgestalt.org). In addition, gene-set enrichment analysis of RNA-seq and Ribo-seq expression data was performed on gene sets from the Hallmark collection in the Molecular Signatures Database.[7]

Sequencing Analysis for Insertion/Deletion Detection

The QIAamp DNA mini kit (Qiagen) was used to extract the total DNA from cells. PCR primers were designed to amplify an approximately 700–base pair region containing the sgRNA cut site, and the PCR product was sent for Sanger sequencing. TIDE (https://tide.deskgen.com/) was used to assess insertion/deletion (indel) frequency of individual sgRNA.[8] The mutation frequency was calculated by dividing the indel percentage by the GFP percentage.

Complementary DNA Mutagenesis and Plasmid Transfection

The pFLAG-CMV2-METTL3 was a kind gift from Prof Richard I. Gregory (Boston Children's Hospital).[9] Q5 Site-Directed Mutagenesis Kit (NEB) was used to generate shMETTL3-2 -resistant form of METTL3 and different METTL3 mutants (aa400-402, IHM/AHM), (aa468-474,

RTGRTGH/RAAAAAH) and (aa477-483, NHGKEHC/AAGAAHA). Sanger sequencing was applied to confirm the sequence of each mutated plasmid. Cells were transfected with expressing plasmids or empty vector using Lipofectamine 2000 (Life Tech).

Glucose Uptake Assay and Lactate Measurement

To measure glucose uptake, cells were incubated with 100 μg/mL 2-deoxy-2-[(7-nitro-2,1,3-benzoxadiazol-4-yl) amino]-D-glucose (2-NBDG, Abcam no. ab235976) in glucose-free medium for 1 hour, and the fluorescence was measured at excitation and emission wavelengths of 485 nm and 535 nm, respectively. The lactate production was measured by using the Lactate Colorimetric/Fluorometric Assay Kit (Abcam no. ab65330) according to the manufacturer's instructions.

Statistical Analysis

All results were expressed as mean ± standard deviation (SD) unless otherwise indicated. To compare the difference between 2 groups, Mann-Whitney *U* test, Wilcoxon matched pairs test, and Student *t* test were performed. The difference between growth rates was determined by ANOVA with repeated-measures analysis of variances. The Pearson chi-square test or Fisher exact test was used for analysis of the associations between patient clinicopathologic characteristics and METTL3 expression. For survival analysis, the follow-up data were truncated at 60 months. The cutoff value of METTL3 mRNA expression in the GSE17536 cohort was analyzed by survival significance analysis by using the tool Cutoff Finder (http://molpath.charite.de/cutoff/). Kaplan-Meier analysis and log rank test were performed to evaluate the association between METTL3 expression and patient survival. The Cox proportion hazard regression model was performed to assess the prognostic value of METTL3 expression. All statistical tests were performed with GraphPad Prism 5.0 (GraphPad Software Inc) or SPSS 20.0 (SPSS Inc), and a 2-tailed *P* value of .05 was considered statistically significant ($*P < .05$, $**P < .01$, $***P < .001$).

References

1. Sato T, Stange DE, Ferrante M, et al. Long-term expansion of epithelial organoids from human colon, adenoma, adenocarcinoma, and Barrett's epithelium. Gastroenterology 2011;141:1762–1772.
2. Langmead B, Trapnell C, Pop M, et al. Ultrafast and memory-efficient alignment of short DNA sequences to the human genome. Genome Biology 2009;10(3):R25.
3. Li W, Xu H, Xiao T, et al. MAGeCK enables robust identification of essential genes from genome-scale CRISPR/Cas9 knockout screens. Genome Biology 2014;15:554.
4. Pan Y, Tong JHM, Lung RWM, et al. RASAL2 promotes tumor progression through LATS2/YAP1 axis of hippo signaling pathway in colorectal cancer. Mol Cancer 2018;17(1):102.
5. **Tang J, Chen H**, Wong CC, et al. DEAD-box helicase 27 promotes colorectal cancer growth and metastasis and predicts poor survival in CRC patients. Oncogene 2018;37:3006–3021.
6. Chen H, Wong CC, Liu D, et al. APLN promotes hepatocellular carcinoma through activating PI3K/Akt pathway and is a druggable target. Theranostics 2019;9:5246–5260.
7. **Subramanian A, Tamayo P**, Mootha VK, et al. Gene set enrichment analysis: a knowledge-based approach for interpreting genome-wide expression profiles. Proc Natl Acad Sci U S A 2005;102:15545–15550.
8. Brinkman EK, Chen T, Amendola M, et al. Easy quantitative assessment of genome editing by sequence trace decomposition. Nucleic Acids Res 2014;42(22):e168.
9. **Lin S, Choe J**, Du P, et al. The m^6A methyltransferase METTL3 promotes translation in human cancer cells. Mol Cell 2016;62:335–345.

Author names in bold designate shared co-first authorship.

Supplementary Table 1. Clinicopathologic Features of METTL3 Expression in Patients With CRC From Hong Kong

Variable	Low METTL3 expression (n = 127)	High METTL3 expression (n = 70)	*P* value
Age, *y*, mean ± SD	67.5 ± 12.1	66.8 ± 12.9	.689
Sex, n (%)			
Male	75 (59.1)	37 (52.9)	.453
Female	52 (40.9)	33 (47.1)	
Tumor location, n (%)			.555
Colon	65 (51.2)	39 (55.7)	
Rectum	62 (48.8)	31 (44.3)	
Tumor size (cm), mean ± SD	4.27 ± 1.75	4.61 ± 1.65	.189
Invasion depth, n (%)			.505
T1, T2	18 (14.2)	7 (10.0)	
T3, T4	109 (85.8)	63 (90.0)	
Lymph node metastasis, n (%)			.768
N0	61 (48.0)	32 (45.7)	
N1, N2	66 (52.0)	38 (54.3)	
Distant metastasis, n (%)			.003
M0	96 (75.6)	38 (54.3)	
M1	31 (24.4)	32 (45.7)	
TNM stage, n (%)			.172
I, II	55 (43.3)	23 (32.9)	
III, IV	72 (56.7)	47 (67.1)	

Supplementary Table 2. Clinicopathologic Features of METTL3 Expression in Patients With CRC From GSE17536

Variable	Low METTL3 expression (n = 109)	High METTL3 expression (n = 68)	*P* value
Age, *y*, mean ± SD	67.0 ± 11.3	63.1 ± 15.3	.053
Sex, n (%)			
Male	57 (52.3)	39 (57.3)	.538
Female	52 (47.7)	29 (42.7)	
Distant metastasis, n (%)			.039
M0	91 (83.5)	47 (69.1)	
M1	18 (16.5)	21 (30.9)	
TNM stage, n (%)			.123
I, II	55 (50.5)	26 (38.2)	
III, IV	54 (49.5)	42 (61.8)	

Supplementary Table 3. Primers List

Primer	For *Mettl3*$^{+/-}$ mice genotyping
Mettl3-F	AAGTGCTGCCATGTGAAT
Mettl3-R1	CATCTTGAGTGGCAGGTG
Mettl3-R2	GAAAGGAGAAGACGATAAGAC
For MeRIP-qPCR	
SLC2A1-F	AGTGACAAGACACCCGAGGA
SLC2A1-R	CCTGTGCTCCTGAGAGATCC
Jun-F	GCCAACTCATGCTAACGCAG
Jun-R	TTCTCTCCGTCGCAACTTGT
PTTG1IP-F	TGTGTGCAAAATCCGCTTCC
PTTG1IP-R	CGACCTTACAGACGTGGGTT
NUAK1-F	ATTTGCAGGAGAATCGCCCT
NUAK1-R	GGTACCGCTTCAGGTACTGG
LAMC2-F	GGGCAATGAGGCAGATAGCA
LAMC2-R	TGCCTGGGCAAAGTCAAAGT
ACTB-F	AGAGCTACGAGCTGCCTGAC
ACTB-R	AGCACTGTGTTGGCGTACAG
For qPCR	
METTL3-F	ATGCTGTGTCCATCTGTCTTGC
METTL3-R	GGAGACCTCGCTTTACCTCAATC
SLC2A1-F	AGTGACAAGACACCCGAGGA
SLC2A1-R	CCTGTGCTCCTGAGAGATCC
ACTB-F	AGAGCTACGAGCTGCCTGAC
ACTB-R	AGCACTGTGTTGGCGTACAG
For site-directed mutagenesis	
M3mut2-F	cacatgGAACTGCCCTATGGGACC
M3mut2-R	agcatcCCAGGGTGGGTCAGCCAT
M3mut3-F	tgcagctcacTGGTTGAACCATGGGAAG
M3mut3-R	gcggctgcccgAATGATGCGTTGCAGTTG
M3mut4-F	ggcacacgccTTGGTTGGTGTCAAAGGAAATC
M3mut4-R	gccccagcggcCAACCAGTGACCTGTACG
For indel detection	
sg3.1-pcr-F	GGCAGCATTGTCTCCAACCT
sg3.1-pcr-R	CCCCTACCTTCTTGCTCTGT
sg6.4 (6.6)-pcr-F	ACCGACTCTTCCCACCTCA
sg6.4 (6.6)-pcr-R	GCATTGTAAACAGGCATTAGGA

Supplementary Table 4. Gene List of Common METTL3 Targets (m^6A-seq)

Transcript	Gene symbol	Transcript	Gene symbol
ENST00000535787	*ACVR2A*	ENST00000396039	*PARD6B*
ENST00000260600	*ADCY3*	ENST00000447133	*PARP11*
ENST00000400822	*AFDN*	ENST00000298281	*PCF11*
ENST00000377698	*ALDH1B1*	ENST00000259467	*PDCL*
ENST00000514516	*AMOTL2*	ENST00000374012	*PHF20*
ENST00000341657	*ANKFY1*	ENST00000409681	*POLR1A*
ENST00000361627	*ARHGAP11A*	ENST00000260970	*PPIG*
ENST00000404338	*ARHGAP35*	ENST00000271526	*PRCC*
ENST00000378115	*ARHGEF35*	ENST00000376588	*PSAT1*
ENST00000557666	*BAG5*	ENST00000445724	*PTTG1IP*
ENST00000538010	*BCL7A*	ENST00000544304	*RAB35*
ENST00000400558	*C21orf91*	ENST00000542104	*RASSF3*
ENST00000418388	*C9orf69*	ENST00000563281	*RBM15B*
ENST00000493278	*CALU*	ENST00000262031	*RBMS2*
ENST00000358823	*CAMSAP2*	ENST00000381249	*RDH14*
ENST00000372927	*CENPI*	ENST00000361070	*RFWD3*
ENST00000361283	*CHAMP1*	ENST00000325875	*RMI1*
ENST00000571457	*CHMP6*	ENST00000399799	*ROCK1*
ENST00000534224	*CREBZF*	ENST00000392067	*SAMD4A*
ENST00000280527	*CRIM1*	ENST00000324679	*SAV1*
ENST00000572145	*CRK*	ENST00000337221	*SCARA3*
ENST00000367976	*CTGF*	ENST00000360820	*SCYL2*
ENST00000471014	*CTNNB1*	ENST00000381150	*SDC1*
ENST00000451137	*CYR61*	ENST00000358171	*SERPINH1*
ENST00000396741	*CYTH3*	ENST00000526638	*SERPINH1*
ENST00000538711	*DAG1*	ENST00000271628	*SF3B4*
ENST00000354185	*DDX21*	ENST00000272542	*SLC20A1*
ENST00000594099	*DNAJB1*	ENST00000381401	*SLC25A6*
ENST00000460191	*DNTTIP2*	ENST00000426263	*SLC2A1*
ENST00000369583	*DUSP5*	ENST00000075120	*SLC2A3*
ENST00000279488	*DUSP6*	ENST00000256689	*SLC38A2*
ENST00000374980	*EIF2S2*	ENST00000556605	*SLC39A9*
ENST00000366844	*ENAH*	ENST00000416247	*SMIM13*
ENST00000510316	*ENC1*	ENST00000298532	*SNAPC4*
ENST00000395673	*EXT2*	ENST00000306503	*SOCS5*
ENST00000591269	*FAM210A*	ENST00000344051	*SPINT1*
ENST00000369756	*FAM46A*	ENST00000367723	*SUCO*
ENST00000239906	*FAM53C*	ENST00000374270	*SUSD1*
ENST00000509647	*FAT1*	ENST00000355585	*SYNJ2*

Supplementary Table 4. Continued

Transcript	Gene symbol	Transcript	Gene symbol
ENST00000618099	*FURIN*	ENST00000612220	*TACC3*
ENST00000215631	*GADD45B*	ENST00000416067	*TEKT4P2*
ENST00000265000	*GALNT7*	ENST00000359013	*TGFBR2*
ENST00000264039	*GPC1*	ENST00000377386	*TGOLN2*
ENST00000626993	*HIPK1*	ENST00000260356	*THBS1*
ENST00000562569	*HN1L*	ENST00000296978	*TMEM200A*
ENST00000313552	*ING5*	ENST00000266712	*TMTC3*
ENST00000374242	*INIP*	ENST00000296861	*TNFRSF21*
ENST00000371222	*JUN*	ENST00000357503	*TOR4A*
ENST00000346991	*KNL1*	ENST00000617904	*TRAPPC3*
ENST00000394815	*KRT80*	ENST00000456197	*TRRAP*
ENST00000258341	*LAMC1*	ENST00000476784	*TTC3*
ENST00000264144	*LAMC2*	ENST00000586691	*TUBB6*
ENST00000341247	*LIMA1*	ENST00000232165	*UBE3A*
ENST00000513071	*LOC101929595*	ENST00000262803	*UPF1*
ENST00000550474	*LOC102724050*	ENST00000540269	*USP10*
ENST00000378251	*LRRC47*	ENST00000614860	*USPL1*
ENST00000464060	*MAGI1*	ENST00000254803	*UTP3*
ENST00000356554	*MAN1A2*	ENST00000559478	*WDR20*
ENST00000416600	*MAVS*	ENST00000407426	*WDR43*
ENST00000261758	*MESDC2*	ENST00000310380	*XXYLT1*
ENST00000453731	*MFSD2B*	ENST00000307630	*YWHAG*
ENST00000494512	*MIS18BP1*	ENST00000397492	*YWHAH*
ENST00000244230	*MPHOSPH10*	ENST00000430430	*ZBTB10*
ENST00000555925	*MPP5*	ENST00000313732	*ZDHHC7*
ENST00000382142	*MTMR12*	ENST00000308683	*ZNF622*
ENST00000621592	*MYC*	ENST00000286067	
ENST00000261797	*NDST1*	ENST00000450443	
ENST00000275820	*NOM1*	ENST00000502978	
ENST00000435510	*NRBF2*	ENST00000559468	
ENST00000261402	*NUAK1*	ENST00000611513	
ENST00000367157	*NUAK2*	ENST00000618004	
ENST00000225388	*NUFIP2*	ENST00000623664	
ENST00000538151	*OCLN*	ENST00000626721	

Supplementary Table 5. m^6A Enrichment of Candidate METTL3 Targets (m^6A-seq)

Gene	Chromosome	Position	NC1 enrichment	NC1 m^6A	NC1 input	SH1 enrichment	SH1 m^6A	SH1 input
SLC2A1	1	4.293E+07	3.02	120	39	1.99	41	20
Jun	1	5.878E+07	7.46	87	11	5.84	10	1
LAMC2	1	1.832E+08	4.85	13	2	NA[a]		
NUAK1	12	1.061E+08	5.91	22	3	NA[a]		
PTTG1IP	21	4.485E+07	4.05	61	15	2.03	23	11

			NC2 enrichment	NC2 m^6A	NC2 input	SH2 enrichment	SH2 m^6A	SH2 input
SLC2A1	1	4.293E+07	2.93	118	40	NA[a]		
Jun	1	5.878E+07	18.07	266	14	16.42	111	6
LAMC2	1	1.832E+08	4.04	11	2	NA[a]		
NUAK1	12	1.061E+08	17.61	16	0	NA[a]		
PTTG1IP	21	4.485E+07	15.51	294	18	10.21	116	11

NA, no identified m^6A peak; NC1, HCT116-shGFP; NC2, DLD1-shGFP; SH1, HCT116-shMETTL3; SH2, DLD1-shMETTL3.
[a]No identified m^6A peak. Read counts are shown for specified regions.

Supplementary Table 6. Significantly Up-regulated and Down-regulated Genes Upon METTL3 Depletion (RNA-Seq)

Transcript	Gene symbol	Log_2 fold change (shMETTL3/ shGFP)	*P* value
ENSG00000165376.10	*CLDN2*	–5.059252248	.005746
ENSG00000202031.1	*SNORD38A*	–4.763961664	.012704
ENSG00000183423.11	*LRIT3*	–4.637010556	.018033
ENSG00000207081.1	*RNU6-616P*	–4.584094274	.01974
ENSG00000261189.1	*AL031058.1*	–4.491380063	.024657
ENSG00000182154.7	*MRPL41*	–4.478576363	.025113
ENSG00000233013.10	*FAM157B*	–4.465679005	.025913
ENSG00000177359.20	*AC024940.1*	–4.378564492	.031476
ENSG00000184967.6	*NOC4L*	–4.364731316	.032305
ENSG00000164398.12	*ACSL6*	–4.225842266	.044165
ENSG00000148200.16	*NR6A1*	–2.770086664	1.15E–15
ENSG00000145703.15	*IQGAP2*	–2.769063667	2.33E–06
ENSG00000104081.13	*BMF*	–2.690958424	.021105
ENSG00000143195.12	*ILDR2*	–2.608179795	.000322
ENSG00000285108.1	*AC103718.1*	–2.468268908	.004896
ENSG00000169733.11	*RFNG*	–2.435403778	.020014
ENSG00000100711.13	*ZFYVE21*	–2.418208816	.000303
ENSG00000151320.10	*AKAP6*	–2.299681712	.001315
ENSG00000068615.18	*REEP1*	–2.251237597	.000629
ENSG00000115604.10	*IL18R1*	–2.169549912	.048886
ENSG00000180914.10	*OXTR*	–2.098024307	.036946
ENSG00000047634.14	*SCML1*	–2.091181588	.008977
ENSG00000100577.18	*GSTZ1*	–2.077088099	.014553
ENSG00000146250.6	*PRSS35*	–2.058197506	.042118
ENSG00000159348.12	*CYB5R1*	–1.993595673	.003579
ENSG00000179750.15	*APOBEC3B*	–1.957704411	.028175
ENSG00000102098.17	*SCML2*	–1.940081684	.00041
ENSG00000273038.2	*AL365203.2*	–1.917680268	.039077
ENSG00000011105.13	*TSPAN9*	–1.899185139	.009641
ENSG00000109099.14	*PMP22*	–1.893045011	.000178
ENSG00000060656.19	*PTPRU*	–1.856253539	5.93E–05
ENSG00000003989.17	*SLC7A2*	–1.830735043	2.00E–06
ENSG00000178445.9	*GLDC*	–1.829491396	.037211
ENSG00000196083.9	*IL1RAP*	–1.779882457	.000751
ENSG00000167600.13	*CYP2S1*	–1.743018673	.008736
ENSG00000119139.19	*TJP2*	–1.733718218	.038691
ENSG00000160201.11	*U2AF1*	–1.733680502	.002636
ENSG00000171617.13	*ENC1*	–1.718406288	4.59E–13
ENSG00000076706.16	*MCAM*	–1.714778516	1.87E–05
ENSG00000181418.7	*DDN*	–1.703790585	.045032
ENSG00000170681.6	*CAVIN4*	–1.691995064	.011424
ENSG00000183508.4	*TENT5C*	–1.639395117	.039505
ENSG00000167772.11	*ANGPTL4*	–1.570633862	.026228
ENSG00000154639.18	*CXADR*	–1.512986112	8.65E–09
ENSG00000139971.15	*ARMH4*	–1.500760425	.027134
ENSG00000163376.11	*KBTBD8*	–1.485313498	.001296
ENSG00000197822.10	*OCLN*	–1.47021676	.000253
ENSG00000162409.10	*PRKAA2*	–1.457112272	7.31E–05
ENSG00000106771.12	*TMEM245*	–1.45161946	1.25E–12
ENSG00000025770.18	*NCAPH2*	–1.445242177	.030786
ENSG00000157470.11	*FAM81A*	–1.438883659	.044745
ENSG00000143061.17	*IGSF3*	–1.43856432	8.79E–07
ENSG00000160233.7	*LRRC3*	–1.435894674	.031716
ENSG00000172795.15	*DCP2*	–1.423815679	7.44E–17
ENSG00000105810.9	*CDK6*	–1.394471806	1.15E–26
ENSG00000151693.10	*ASAP2*	–1.390021552	6.09E–05
ENSG00000135269.17	*TES*	–1.38369246	1.08E–13
ENSG00000135862.5	*LAMC1*	–1.371014263	2.69E–25
ENSG00000135678.11	*CPM*	–1.359828642	.026362
ENSG00000174938.14	*SEZ6L2*	–1.344647475	.034525
ENSG00000162490.6	*DRAXIN*	–1.325844235	.013396
ENSG00000165959.11	*CLMN*	–1.315736204	1.14E–05
ENSG00000259820.1	*AC083843.2*	–1.314662423	.002816
ENSG00000166145.14	*SPINT1*	–1.309244646	.000472
ENSG00000117394.21	*SLC2A1*	–1.306621693	7.02E–12
ENSG00000201592.1	*RF00494*	–1.297265402	.030135
ENSG00000101928.12	*MOSPD1*	–1.290282211	1.58E–06
ENSG00000064300.8	*NGFR*	–1.288780882	.025318
ENSG00000105409.18	*ATP1A3*	–1.283429795	.035656
ENSG00000120885.21	*CLU*	–1.280161277	5.36E–10
ENSG00000239264.8	*TXNDC5*	–1.260216411	.024028
ENSG00000035403.17	*VCL*	–1.250574998	2.12E–18

Supplementary Table 6. Continued

Transcript	Gene symbol	Log_2 fold change (shMETTL3/ shGFP)	*P* value
ENSG00000147231.13	*CXorf57*	−1.243074389	.032543
ENSG00000166831.8	*RBPMS2*	−1.239626575	.032118
ENSG00000197168.12	*NEK5*	−1.239536435	.021776
ENSG00000095739.10	*BAMBI*	−1.233689998	.026829
ENSG00000185950.8	*IRS2*	−1.232841496	.048971
ENSG00000169991.10	*IFFO2*	−1.216455912	.004476
ENSG00000091409.14	*ITGA6*	−1.215277426	7.90E–24
ENSG00000121743.3	*GJA3*	−1.205629191	.032243
ENSG00000100600.14	*LGMN*	−1.203078724	.004188
ENSG00000276672.1	*AL161891.1*	−1.181571973	.005963
ENSG00000112773.15	*TENT5A*	−1.178573639	1.82E–06
ENSG00000115652.14	*UXS1*	−1.177546643	1.92E–09
ENSG00000165757.8	*JCAD*	−1.175675762	4.46E–07
ENSG00000186480.12	*INSIG1*	−1.174021625	.00011
ENSG00000171365.16	*CLCN5*	−1.172298389	.013577
ENSG00000072958.8	*AP1M1*	−1.161790028	.039447
ENSG00000180667.10	*YOD1*	−1.156955884	.000124
ENSG00000165490.12	*DDIAS*	−1.154689967	.003311
ENSG00000116745.6	*RPE65*	−1.1470539	.020242
ENSG00000106615.9	*RHEB*	−1.144688466	.023362
ENSG00000196569.12	*LAMA2*	−1.142535677	.012717
ENSG00000147475.15	*ERLIN2*	−1.138393661	6.99E–05
ENSG00000206418.4	*RAB12*	−1.136057128	1.29E–06
ENSG00000063660.8	*GPC1*	−1.135436186	.006876
ENSG00000171444.17	*MCC*	−1.116625409	.000406
ENSG00000131746.12	*TNS4*	−1.115168316	.016358
ENSG00000112378.11	*PERP*	−1.111989914	3.04E–09
ENSG00000111665.11	*CDCA3*	−1.104463133	.015287
ENSG00000100473.16	*COCH*	−1.103023231	.041089
ENSG00000162433.14	*AK4*	−1.100784094	3.81E–09
ENSG00000164086.9	*DUSP7*	−1.097973273	.004864
ENSG00000168785.7	*TSPAN5*	−1.095963867	2.39E–07
ENSG00000141956.13	*PRDM15*	−1.093990866	.003221
ENSG00000184203.7	*PPP1R2*	−1.092902145	2.47E–07
ENSG00000055732.12	*MCOLN3*	−1.088572549	.023842
ENSG00000205189.11	*ZBTB10*	−1.078625659	1.77E–08
ENSG00000151240.16	*DIP2C*	−1.074876058	.008225

Supplementary Table 6. Continued

Transcript	Gene symbol	Log_2 fold change (shMETTL3/ shGFP)	*P* value
ENSG00000186866.16	*POFUT2*	−1.074400336	.003552
ENSG00000165609.12	*NUDT5*	−1.072520291	8.04E–05
ENSG00000179820.15	*MYADM*	−1.072033472	.011247
ENSG00000160256.12	*FAM207A*	−1.07059944	.035509
ENSG00000104635.13	*SLC39A14*	−1.070441444	4.06E–07
ENSG00000051825.14	*MPHOSPH9*	−1.070202723	7.69E–07
ENSG00000179134.15	*SAMD4B*	−1.067926515	.007889
ENSG00000114019.14	*AMOTL2*	−1.066809551	.017653
ENSG00000171848.14	*RRM2*	−1.065951946	6.87E–21
ENSG00000106484.15	*MEST*	−1.064832286	.041719
ENSG00000165650.11	*PDZD8*	−1.063695826	4.39E–14
ENSG00000123908.11	*AGO2*	−1.059707364	2.33E–15
ENSG00000204388.6	*HSPA1B*	−1.05901595	1.31E–05
ENSG00000101384.12	*JAG1*	−1.058523233	9.91E–06
ENSG00000092208.17	*GEMIN2*	−1.051472407	.024457
ENSG00000107614.21	*TRDMT1*	−1.050840458	.031149
ENSG00000151725.11	*CENPU*	−1.050043949	4.24E–05
ENSG00000164236.11	*ANKRD33B*	−1.045016845	.001292
ENSG00000173258.12	*ZNF483*	−1.032243742	.009587
ENSG00000093009.9	*CDC45*	−1.032176525	.038624
ENSG00000067955.13	*CBFB*	−1.031361568	2.45E–09
ENSG00000186141.8	*POLR3C*	−1.027725224	.016523
ENSG00000197930.12	*ERO1A*	−1.027370632	6.03E–06
ENSG00000183605.16	*SFXN4*	−1.021135593	.028615
ENSG00000155846.16	*PPARGC1B*	−1.020817517	.018644
ENSG00000006327.13	*TNFRSF12A*	−1.019468293	.018735
ENSG00000224531.5	*SMIM13*	−1.018346072	.004905
ENSG00000075826.16	*SEC31B*	−1.018008053	.017138
ENSG00000164674.15	*SYTL3*	−1.016287437	.021269
ENSG00000049130.15	*KITLG*	−1.014709449	2.96E–34
ENSG00000141449.14	*GREB1L*	−1.014295659	.001228
ENSG00000197321.14	*SVIL*	−1.012469768	6.19E–07
ENSG00000109452.12	*INPP4B*	−1.011692022	.005194
ENSG00000092931.11	*MFSD11*	−1.011497868	.040102
ENSG00000277075.2	*HIST1H2AE*	1.000354917	.00232
ENSG00000277161.1	*PIGW*	1.008586862	.037014
ENSG00000135480.15	*KRT7*	1.011382772	.005915

Supplementary Table 6. Continued

Transcript	Gene symbol	Log_2 fold change (shMETTL3/ shGFP)	*P* value
ENSG00000073711.10	*PPP2R3A*	1.017669081	.00381
ENSG00000170558.8	*CDH2*	1.019138931	.017992
ENSG00000007968.6	*E2F2*	1.020829963	.020234
ENSG00000142408.4	*CACNG8*	1.025212707	.025939
ENSG00000114446.4	*IFT57*	1.025865395	2.51E–05
ENSG00000117151.12	*CTBS*	1.038034497	.040326
ENSG00000157657.14	*ZNF618*	1.039977517	.00471
ENSG00000131171.12	*SH3BGRL*	1.042863009	4.93E–05
ENSG00000196975.15	*ANXA4*	1.052572039	.00153
ENSG00000285053.1	*TBCE*	1.067657016	.000407
ENSG00000161013.16	*MGAT4B*	1.069548515	.030733
ENSG00000177732.8	*SOX12*	1.070171115	.046546
ENSG00000071564.14	*TCF3*	1.074164002	5.14E–05
ENSG00000107537.13	*PHYH*	1.082423177	.039835
ENSG00000171992.12	*SYNPO*	1.092304096	.030527
ENSG00000165832.5	*TRUB1*	1.108046773	2.56E–06
ENSG00000119401.10	*TRIM32*	1.116433411	.009083
ENSG00000197635.9	*DPP4*	1.118279656	.003028
ENSG00000232531.3	*AC027612.3*	1.121920538	.017765
ENSG00000169925.16	*BRD3*	1.125188274	.000581
ENSG00000007047.14	*MARK4*	1.134221019	.000862
ENSG00000169136.10	*ATF5*	1.134902695	.031046
ENSG00000156860.15	*FBRS*	1.137030742	.015861
ENSG00000102870.5	*ZNF629*	1.139991309	9.77E–05
ENSG00000111328.6	*CDK2AP1*	1.147739275	5.04E–07
ENSG00000132470.13	*ITGB4*	1.152574736	1.00E–07
ENSG00000185015.7	*CA13*	1.162159577	.021657
ENSG00000088836.13	*SLC4A11*	1.16626072	.046512
ENSG00000010219.13	*DYRK4*	1.168833977	.032976
ENSG00000013364.18	*MVP*	1.174115977	.016765
ENSG00000083290.19	*ULK2*	1.180444561	.034304
ENSG00000060982.14	*BCAT1*	1.185647689	2.87E–05
ENSG00000268093.1	*AC022154.1*	1.192331596	.021381
ENSG00000161714.11	*PLCD3*	1.192589507	.003949
ENSG00000107731.12	*UNC5B*	1.196707017	.000523
ENSG00000171604.11	*CXXC5*	1.197288128	.034183
ENSG00000083307.11	*GRHL2*	1.199129938	.001308

Supplementary Table 6. Continued

Transcript	Gene symbol	Log_2 fold change (shMETTL3/ shGFP)	*P* value
ENSG00000196295.11	*GARS-DT*	1.204886282	.000959
ENSG00000255874.2	*LINC00346*	1.222244099	.048692
ENSG00000082014.16	*SMARCD3*	1.233137144	.016635
ENSG00000203499.11	*IQANK1*	1.264068391	.000559
ENSG00000213462.4	*ERV3-1*	1.270232639	.039018
ENSG00000115129.13	*TP53I3*	1.274645441	.043002
ENSG00000143891.16	*GALM*	1.275565655	.03242
ENSG00000109089.7	*CDR2L*	1.293000821	8.44E–06
ENSG00000259848.8	*AC097374.1*	1.295604264	.044667
ENSG00000142173.14	*COL6A2*	1.301505818	.014562
ENSG00000105559.11	*PLEKHA4*	1.306470777	.003607
ENSG00000180096.11	*Sep1*	1.311292343	.037767
ENSG00000123989.13	*CHPF*	1.3149688	.019162
ENSG00000071967.11	*CYBRD1*	1.345344144	.002099
ENSG00000109654.14	*TRIM2*	1.368440953	5.36E–05
ENSG00000271254.6	*AC240274.1*	1.374919472	.028023
ENSG00000163694.14	*RBM47*	1.399421577	.02258
ENSG00000063180.8	*CA11*	1.425962228	1.80E–06
ENSG00000272398.5	*CD24*	1.441534934	.016892
ENSG00000108846.15	*ABCC3*	1.448963578	.012231
ENSG00000109511.11	*ANXA10*	1.459092249	1.35E–07
ENSG00000110852.4	*CLEC2B*	1.470625409	.030205
ENSG00000172086.7	*KRCC1*	1.474562464	.001914
ENSG00000148848.14	*ADAM12*	1.502978131	.007918
ENSG00000166741.7	*NNMT*	1.50964472	.036561
ENSG00000088340.15	*FER1L4*	1.513219835	.005394
ENSG00000164687.10	*FABP5*	1.51327198	3.07E–27
ENSG00000196154.11	*S100A4*	1.529493711	.007822
ENSG00000165449.11	*SLC16A9*	1.541809588	.020249
ENSG00000144452.14	*ABCA12*	1.544699467	.04382
ENSG00000105053.10	*VRK3*	1.548993576	.020391
ENSG00000168453.14	*HR*	1.559188285	.034146
ENSG00000108244.16	*KRT23*	1.571118753	.025675
ENSG00000258891.1	*AC005480.1*	1.571871085	.039634
ENSG00000136531.15	*SCN2A*	1.572415538	.04637
ENSG00000171033.12	*PKIA*	1.58294022	.032784
ENSG00000131370.15	*SH3BP5*	1.588600338	.02765

Supplementary Table 6. Continued

Transcript	Gene symbol	Log_2 fold change (shMETTL3/ shGFP)	*P* value
ENSG00000261949.5	*GFY*	1.601458845	.041667
ENSG00000153993.13	*SEMA3D*	1.601557019	.045205
ENSG00000221930.6	*FAM45BP*	1.611162972	.045603
ENSG00000276334.1	*AL133243.2*	1.626375116	.03483
ENSG00000186409.15	*CCDC30*	1.629226468	.024298
ENSG00000166446.14	*CDYL2*	1.63301857	.034753
ENSG00000196782.12	*MAML3*	1.651104784	.021583
ENSG00000010704.18	*HFE*	1.711796777	.041759
ENSG00000272599.2	*AC016394.1*	1.753079331	.038071
ENSG00000180543.4	*TSPYL5*	1.778340524	.040788
ENSG00000155066.15	*PROM2*	1.780101357	.014782
ENSG00000152763.16	*WDR78*	1.786227059	.008049
ENSG00000006756.15	*ARSD*	1.789680243	.039675
ENSG00000198203.9	*SULT1C2*	1.799053579	.048831
ENSG00000229089.8	*ANKRD20A8P*	1.814475545	.041889
ENSG00000276386.1	*CNTNAP3P2*	1.820032687	.046009
ENSG00000184922.13	*FMNL1*	1.844448432	.038926
ENSG00000072952.18	*MRVI1*	1.886174389	.010501
ENSG00000114805.17	*PLCH1*	1.903260331	.016297
ENSG00000234964.4	*FABP5P7*	1.928327492	.001276
ENSG00000065618.19	*COL17A1*	1.928868407	.000594
ENSG00000161642.17	*ZNF385A*	1.934652403	.000622
ENSG00000171951.4	*SCG2*	1.941539378	1.37E–07
ENSG00000117318.8	*ID3*	1.943758732	.02412
ENSG00000107159.12	*CA9*	1.94619421	.033291
ENSG00000185565.11	*LSAMP*	1.980909896	.007817
ENSG00000104723.20	*TUSC3*	1.988098989	.024944
ENSG00000003147.18	*ICA1*	1.999951684	.004792
ENSG00000237512.6	*UNC5B-AS1*	2.098585752	.041223
ENSG00000282772.1	*AL358790.1*	2.107863495	.010258
ENSG00000170500.12	*LONRF2*	2.138645366	.001414
ENSG00000272812.1	*AC004908.2*	2.18876173	.041533
ENSG00000205583.13	*STAG3L1*	2.191159696	.047562
ENSG00000213514.2	*AL731556.1*	2.208012242	.026233
ENSG00000154165.4	*GPR15*	2.221403254	.015689
ENSG00000125864.13	*BFSP1*	2.236823183	.000377
ENSG00000280614.1	*FP236383.2*	2.262718198	.001773

Supplementary Table 6. Continued

Transcript	Gene symbol	Log_2 fold change (shMETTL3/ shGFP)	*P* value
ENSG00000129675.15	*ARHGEF6*	2.277527575	.031295
ENSG00000172403.10	*SYNPO2*	2.348553566	.03958
ENSG00000165591.6	*FAAH2*	2.349930019	.017597
ENSG00000205571.13	*SMN2*	2.461554311	.002082
ENSG00000123009.4	*NME2P1*	2.515517718	.00485
ENSG00000227540.1	*DNAJC9-AS1*	2.604415826	.035389
ENSG00000114378.16	*HYAL1*	2.604769216	.034252
ENSG00000253320.6	*AZIN1-AS1*	2.60781985	.037069
ENSG00000253210.1	*AC040970.1*	2.631790532	.014941
ENSG00000174469.21	*CNTNAP2*	2.656823425	.02879
ENSG00000278416.1	*PMS2P2*	2.789964072	.039981
ENSG00000274964.1	*AC026356.1*	3.01076709	.020764
ENSG00000127152.17	*BCL11B*	3.01214618	.021626
ENSG00000154874.15	*CCDC144B*	3.043835035	.007294
ENSG00000153253.16	*SCN3A*	3.097172854	.046554
ENSG00000259431.5	*THTPA*	3.097172854	.046554
ENSG00000210839.1	*RNU6ATAC5P*	3.11244445	.017186
ENSG00000261654.1	*AL360270.2*	3.235921105	.03417
ENSG00000106991.13	*ENG*	3.361819892	.025091
ENSG00000104490.17	*NCALD*	3.362467846	.026591
ENSG00000240875.5	*LINC00886*	3.441166947	.023119
ENSG00000108924.13	*HLF*	3.441599106	.020132
ENSG00000187634.11	*SAMD11*	3.476385283	.017478
ENSG00000181741.7	*FDX1P1*	3.477614807	.018615
ENSG00000099251.14	*HSD17B7P2*	4.1081727	.028768
ENSG00000245556.2	*SCAMP1-AS1*	4.672910557	.007405

Supplementary Table 7. Significantly Up-regulated and Down-regulated Genes Upon METTL3 Depletion (Ribo-Seq)

	Gene symbol	Log2 fold change (shMETTL3/shGFP)	FDR
ENSG00000175203.15	*DCTN2*	–2.906890596	0.037569721
ENSG00000145817.17	*YIPF5*	–2.624490865	0.038414728
ENSG00000213280.2	*AC090114.1*	–2.584962501	0.061191781
ENSG00000234565.1	*COX6B1P1*	–2.523561956	0.056774775
ENSG00000214012.4	*KRT18P38*	–2.478047297	0.08859634
ENSG00000214207.2	*KRT18P10*	–2.459431619	0.014673216
ENSG00000124357.13	*NAGK*	–2.237039197	0.05770546
ENSG00000132692.19	*BCAN*	–2.137503524	0.009545554
ENSG00000186895.4	*FGF3*	–2.131244533	0.049324878
ENSG00000119969.15	*HELLS*	–2.078002512	0.033906408
ENSG00000102103.16	*PQBP1*	–2.070389328	0.094720741
ENSG00000142920.17	*AZIN2*	–2.00413973	0.015931844
ENSG00000240912.1	*AC092896.1*	–1.974004791	0.018790904
ENSG00000138081.20	*FBXO11*	–1.95419631	0.095472937
ENSG00000185164.14	*NOMO2*	–1.938599455	0.07092156
ENSG00000158406.4	*HIST1H4H*	–1.925999419	0.019853532
ENSG00000217130.1	*AL139100.1*	–1.906890596	0.059487937
ENSG00000141101.13	*NOB1*	–1.902702799	0.032979115
ENSG00000118004.17	*COLEC11*	–1.893084796	0.062020091
ENSG00000117394.21	*SLC2A1*	–1.863118194	0.024247491
ENSG00000278272.1	*HIST1H3C*	–1.852442812	0.05120124
ENSG00000161654.9	*LSM12*	–1.836501268	0.064452763
ENSG00000148204.12	*CRB2*	–1.828233652	0.013013102
ENSG00000159111.13	*MRPL10*	–1.807354922	0.040892501
ENSG00000117984.14	*CTSD*	–1.768408642	0.02227021
ENSG00000107821.14	*KAZALD1*	–1.767934572	0.020710965
ENSG00000141552.17	*ANAPC11*	–1.678071905	0.098377455
ENSG00000144354.14	*CDCA7*	–1.637429921	0.079974269
ENSG00000071539.14	*TRIP13*	–1.628031223	0.041689119
ENSG00000130309.11	*COLGALT1*	–1.621488377	0.055833137
ENSG00000050405.13	*LIMA1*	–1.584962501	0.07172811
ENSG00000233270.1	*SNRPEP4*	–1.544320516	0.082329904
ENSG00000198842.9	*DUSP27*	–1.523561956	0.035772515
ENSG00000178631.7	*ACTG1P1*	–1.509013647	0.081526201
ENSG00000224094.1	*RPS24P8*	–1.509013647	0.093959581
ENSG00000180198.16	*RCC1*	–1.478047297	0.067725581
ENSG00000240950.1	*AC021074.1*	–1.476438044	0.032192014
ENSG00000175221.15	*MED16*	–1.473931188	0.096210841
ENSG00000198561.13	*CTNND1*	–1.459431619	0.045653377

Supplementary Table 7. Continued

	Gene symbol	Log2 fold change (shMETTL3/shGFP)	FDR
ENSG00000248159.1	*HSPA8P11*	–1.428843299	0.076790738
ENSG00000127241.16	*MASP1*	–1.424497829	0.087813194
ENSG00000162704.16	*ARPC5*	–1.367731785	0.068530546
ENSG00000232394.1	*AC090696.1*	–1.338801913	0.062836691
ENSG00000276410.3	*HIST1H2BB*	–1.311201688	0.053983835
ENSG00000260908.1	*AC009093.3*	–1.30256277	0.047373968
ENSG00000109919.10	*MTCH2*	–1.275634443	0.084704801
ENSG00000261716.2	*AC239868.1*	–1.272252936	0.069319003
ENSG00000187051.9	*RPS19BP1*	–1.271302022	0.097654669
ENSG00000223345.3	*HIST2H2BA*	–1.256013978	0.046418034
ENSG00000226908.1	*HIST1H2BPS3*	–1.243925583	0.090132379
ENSG00000233155.1	*HMGA1P8*	–1.234465254	0.07342118
ENSG00000120686.12	*UFM1*	–1.213595473	0.050281968
ENSG00000114391.13	*RPL24*	–1.209453366	0.075965004
ENSG00000074590.13	*NUAK1*	–1.191141487	0.080757307
ENSG00000196787.3	*HIST1H2AG*	–1.176644599	0.09244317
ENSG00000089248.7	*ERP29*	–1.137503524	0.090899782
ENSG00000275895.7	*U2AF1L5*	–1.102361718	0.078389126
ENSG00000163132.7	*MSX1*	–1.087462841	0.091676537
ENSG00000170004.16	*CHD3*	2.079727192	0.079176608
ENSG00000155158.20	*TTC39B*	2.121990524	0.063640307
ENSG00000169181.13	*GSG1L*	2.192645078	0.054916193
ENSG00000198807.12	*PAX9*	2.209453366	0.077596303
ENSG00000155816.20	*FMN2*	2.216317907	0.053035917
ENSG00000183955.13	*KMT5A*	2.230297619	0.093196827
ENSG00000068078.18	*FGFR3*	2.268488836	0.070101146
ENSG00000129968.15	*ABHD17A*	2.273018494	0.072564344
ENSG00000197948.11	*FCHSD1*	2.339850003	0.089366227
ENSG00000111218.11	*PRMT8*	2.354842717	0.034856891
ENSG00000116254.18	*CHD5*	2.360747344	0.040056814
ENSG00000173338.12	*KCNK7*	2.36923381	0.058611777
ENSG00000123405.14	*NFE2*	2.376375879	0.099099476
ENSG00000107140.16	*TESK1*	2.38466385	0.065292348
ENSG00000079313.15	*REXO1*	2.38466385	0.06692115
ENSG00000085063.16	*CD59*	2.392317423	0.083920851
ENSG00000185811.18	*IKZF1*	2.459431619	0.025359122
ENSG00000046889.19	*PREX2*	2.459431619	0.066114583
ENSG00000178919.8	*FOXE1*	2.473931188	0.087041004
ENSG00000150995.19	*ITPR1*	2.50779464	0.060348415

Supplementary Table 7. Continued

	Gene symbol	Log2 fold change (shMETTL3/shGFP)	FDR
ENSG00000205189.12	*ZBTB10*	2.560714954	0.027413865
ENSG00000175768.13	*TOMM5*	2.654004145	0.024790079
ENSG00000230393.1	*AC092667.1*	2.678071905	0.085480528
ENSG00000156218.13	*ADAMTSL3*	2.716207034	0.048350803
ENSG00000135314.12	*KHDC1*	2.736965594	0.099817643
ENSG00000148488.17	*ST8SIA6*	2.744161096	0.011217266
ENSG00000128881.17	*TTBK2*	2.7589919	0.026485584
ENSG00000164687.11	*FABP5*	2.760812336	0.031343203
ENSG00000268996.3	*MAN1B1-DT*	2.765534746	0.09693733
ENSG00000144040.12	*SFXN5*	2.830074999	0.074275264
ENSG00000100027.15	*YPEL1*	2.836501268	0.029453282
ENSG00000138777.20	*PPA2*	2.847996907	0.021525957
ENSG00000187824.8	*TMEM220*	2.963474124	0.044881361
ENSG00000136867.11	*SLC31A2*	2.971985624	0.044072612
ENSG00000169840.4	*GSX1*	2.984893108	0.028462367
ENSG00000001460.18	*STPG1*	3	0.052115485
ENSG00000259308.3	*AC024270.1*	3.050626073	0.022963749
ENSG00000157693.15	*TMEM268*	3.142957954	0.0432534
ENSG00000135100.17	*HNF1A*	3.222392421	0.086256573
ENSG00000105607.13	*GCDH*	3.232660757	0.025927731
ENSG00000272841.1	*AL139393.2*	3.350497247	0.042449135
ENSG00000236044.1	*FABP5P2*	3.40599236	0.023649334
ENSG00000240122.1	*FABP5P11*	3.421463768	0.039233204
ENSG00000274993.1	*AC254629.1*	3.426264755	0.036684869
ENSG00000234964.4	*FABP5P7*	3.781359714	0.004862868
ENSG00000147813.16	*NAPRT*	3.790076931	0.017463163
ENSG00000239899.3	*RN7SL674P*	3.906890596	0.083125676
ENSG00000241735.2	*FABP5P3*	4.169925001	0.030424489
ENSG00000106025.8	*TSPAN12*	4.807354922	0.075125373

Supplementary Table 8. Sequences of METTL3 sgRNAs for CRISPR Domain–Targeting Assay

Name	Forward (5′–3′)	Reverse (5′–3′)
M3sg1.1	CACCGGGACACGTGGAGCTCTATCC	AAACGGATAGAGCTCCACGTGTCCC
M3sg2.1	CACCGGGGCTGTCACTACGGAAGGT	AAACACCTTCCGTAGTGACAGCCCC
M3sg2.2	CACCGCACTGGGCTGTCACTACGGA	AAACTCCGTAGTGACAGCCCAGTGC
M3sg2.3	CACCGTCAGGATCTGTAGCTAATTC	AAACGAATTAGCTACAGATCCTGAC
M3sg2.4	CACCGGCTACACCACCTCTCTGATC	AAACGATCAGAGAGGTGGTGTAGCC
M3sg3.1	CACCGTCTACCCCATCTTGAGTGGC	AAACGCCACTCAAGATGGGGTAGAC
M3sg3.2	CACCGGAGTTGATTGAGGTAAAGCG	AAACCGCTTTACCTCAATCAACTCC
M3sg3.3	CACCGTCAGCATAGGTTACAAGAGT	AAACACTCTTGTAACCTATGCTGAC
M3sg3.4	CACCGGCAGAAGCGGCGTGCAGAAC	AAACGTTCTGCACGCCGCTTCTGCC
M3sg3.5	CACCGCAGACCAGAGACTAACGAAC	AAACGTTCGTTAGTCTCTGGTCTGC
M3sg3.6	CACCGTTTGCCAGTTCGTTAGTCTC	AAACGAGACTAACGAACTGGCAAAC
M3sg3.7	CACCGTTCAGCATCGGAACCAGCAA	AAACTTGCTGGTTCCGATGCTGAAC
M3sg3.8	CACCGTGCTGCCTCAGATGTTGATC	AAACGATCAACATCTGAGGCAGCAC
M3sg3.9	CACCGTCTGAACCAACAGTCCACTA	AAACTAGTGGACTGTTGGTTCAGAC
M3sg4.1	CACCGGTTGAAAAATTTCGCTCTCG	AAACCGAGAGCGAAATTTTTCAACC
M3sg4.2	CACCGAAAAATTTCGCTCTCGAGGT	AAACACCTCGAGAGCGAAATTTTTC
M3sg4.3	CACCGAAAATTTCGCTCTCGAGGTC	AAACGACCTCGAGAGCGAAATTTTC
M3sg4.4	CACCGACAGGGTCGATCAGCATCAC	AAACGTGATGCTGATCGACCCTGTC
M3sg4.5	CACCGCTGAAGTGCAGCTTGCGACA	AAACTGTCGCAAGCTGCACTTCAGC
M3sg6.2	CACCGTGCCCAAGATACTGACGTCC	AAACGGACGTCAGTATCTTGGGCAC
M3sg6.3	CACCGTACCTGGACGTCAGTATCTT	AAACAAGATACTGACGTCCAGGTAC
M3sg6.4	CACCGTTGTGATGGCTGACCCACCC	AAACGGGTGGGTCAGCCATCACAAC
M3sg6.5	CACCGATTCACATGGAACTGCCCTA	AAACTAGGGCAGTTCCATGTGAATC
M3sg6.6	CACCGTCATCTGTCAGGGTCCCATA	AAACTATGGGACCCTGACAGATGAC
M3sg6.7	CACCGTGCGCATCTCATCATCTGTC	AAACGACAGATGATGAGATGCGCAC
M3sg6.8	CACCGTGACAGATGATGAGATGCGC	AAACGCGCATCTCATCATCTGTCAC
M3sg6.9	CACCGAAGCCATCATCCTGTAGTAC	AAACGTACTACAGGATGATGGCTTC
M3sg6.10	CACCGGCTCAACATACCCGTACTAC	AAACGTAGTACGGGTATGTTGAGCC
M3sg6.11	CACCGATACCCGTACTACAGGATGA	AAACTCATCCTGTAGTACGGGTATC
M3sg8.1	CACCGATCAACTGCAACGCATCATT	AAACAATGATGCGTTGCAGTTGATC
M3sg8.3	CACCGATCATTCGGACAGGCCGTAC	AAACGTACGGCCTGTCCGAATGATC
M3sg8.4	CACCGGGTTCAACCAGTGACCTGTA	AAACTACAGGTCACTGGTTGAACCC
M3sg8.5	CACCGGGACAGGCCGTACAGGTCAC	AAACGTGACCTGTACGGCCTGTCCC
M3sg8.6	CACCGCAGGTCACTGGTTGAACCAT	AAACATGGTTCAACCAGTGACCTGC
M3sg9.1	CACCGAAATCCCCAAGGCTTCAACC	AAACGGTTGAAGCCTTGGGGATTTC
M3sg10.1	CACCGAACTCAATCTTGCGAGTGCC	AAACGGCACTCGCAAGATTGAGTTC
M3sg10.2	CACCGCAGTTGGGTTGCACATTGTG	AAACCACAATGTGCAACCCAACTGC
M3sg11.1	CACCGGTAGGTGGATCCCATCCAGT	AAACACTGGATGGGATCCACCTACC
M3sg11.2	CACCGCAACCACATCTGGGTCTAGT	AAACACTAGACCCAGATGTGGTTGC

Supplementary Table 8. Continued

Name	Forward (5′–3′)	Reverse (5′–3′)
M3sg11.3	CACCGTTGAACCGTGCAACCACATC	AAACGATGTGGTTGCACGGTTCAAC
M3sg11.4	CACCGTGGTTGCACGGTTCAAGCAA	AAACTTGCTTGAACCGTGCAACCAC
M3sg11.5	CACCGGGTTTAGAGATGATACCATC	AAACGATGGTATCATCTCTAAACCC
Neg1	CACCGGAAGATGGGCGGGAGTCTTC	AAACGAAGACTCCCGCCCATCTTCC